AFRL-VS-HA-TR-98-0081

WAVE PROPAGATION IN THE ARABIAN PLATE

R. B. Herrmann, T. A. Mokhtar, T.-M. Chang, C. J. Ammon and H. A. A. Ghalib

Department of Earth and Atmospheric Sciences
St. Louis University
3507 Laclede Avenue
St. Louis, MO 63103

28 June 1998

Final Report
11 August 1995 - 31 March 1998

DEPARTMENT OF ENERGY
Office of Non-Proliferation
and National Security
WASHINGTON, DC 20585

20000920 058

AIR FORCE RESEARCH LABORATORY
Space Vehicles Directorate
AIR FORCE MATERIEL COMMAND
HANSCOM AIR FORCE BASE, MA 01731-3010

DTIC QUALITY INSPECTED 4

REPORT DOCUMENTATION PAGE

1. AGENCY USE ONLY *(Leave blank)*	2. REPORT DATE 28 June 1998	3. REPORT TYPE AND DATES COVERED Final Report 11 AUG 95 – 31 MAR 98

4. TITLE AND SUBTITLE
Wave Propagation in the Arabian Plate

5. FUNDING NUMBERS
F19628-95-K-0019

PE 69120H
PR DENN
TA GM
WU AJ

6. AUTHOR(S)

R.B. Herrmann, T.A. Mokhtar, T.M. Chang,
C.J. Ammon and H.A. Ghalib

7. PERFORMING ORGANIZATION NAME(S) AND ADDRESS(ES)

Department of Earth and Atmospheric Sciences
Saint Louis University
3507 Laclede
St. Louis, MO 63103

8. PERFORMING ORGANIZATION REPORT NUMBER

9. SPONSORING/MONITORING AGENCY NAME(S) AND ADDRESS(ES)
Air Force Research Laboratory
29 Randolph Road
Hanscom AFB, MA 01731-3010
Contract Manager: Katharine Kadinsky-Cade/VSBS

10. SPONSORING/MONITORING AGENCY REPORT NUMBER

AFRL-VS-HA-TR-98-0081

11. SUPPLEMENTARY NOTES
This research was sponsored by the Department of Energy, Office of Non-Proliferation and National Security, Washington, DC 20585

12a. DISTRIBUTION/AVAILABILITY STATEMENT

Approved for Public Release, Distribution Unlimited

12b. DISTRIBUTION CODE

13. ABSTRACT *(Maximum 200 words)*

This report presents a tomographic analysis of surface-wave group velocity dispersion through the Arabian Plate and studies on the usefulness of genetic algorithms for the inversion of surface-wave waveforms for earth structure.

The raw group velocity dispersion measurements are available by anonymous ftp to ftp.eas.slu.edu in the directory pub/rbh/ARABIA.

14. SUBJECT TERMS
Arabian Plate, Surface Waves, Genetic algorithm, Wave form modeling

15. NUMBER OF PAGES

16. PRICE CODE

17. SECURITY CLASSIFICATION OF REPORT Unclassified	18. SECURITY CLASSIFICATION OF THIS PAGE Unclassified	19. SECURITY CLASSIFICATION OF ABSTRACT Unclassified	20. LIMITATION OF ABSTRACT SAR

CONTENTS

1. LITHOSPHERIC STRUCTURE BENEATH ARABIA

T. A. Mokhtar, C. J. Ammon, R. B. Herrmann, and H. A. A. Ghalib

1.1 Abstract

The three-dimensional seismic velocity distribution beneath the Arabian Plate is investigated using Love and Rayleigh waves. We obtained a balanced path coverage using seismograms generated by earthquakes located along the plate boundaries in the Red Sea, Gulf of Aqaba, Gulf of Aden, western Iran, Turkey, and the Dead Sea fault system. We measured Love- and Rayleigh-wave group velocity dispersion using multiple-filter analysis and then performed a tomographic inversion using these observations to estimate lateral group-velocity variations in the period range of 5-60 seconds. The Love- and Rayleigh-wave results are consistent and show that the average group velocity increases from 2.38 and 2.44 km/s at 5-7 seconds to 3.74 and 3.98 at 56-60 seconds, for Rayleigh and Love waves respectively. The tomographic results also delineate first-order regional structure heterogeneity as well as a sharp transition between the two major tectonic provinces in the region, the Arabian Shield (faster than average) and the Arabian Platform (lower than average).

1.2 Introduction

The deployment of broadband seismic stations within the Arabian Shield (Vernon and Berger, 1997) provided an excellent opportunity to study the seismic structure of the Arabian plate using high-quality seismic signals that were not previously available for this part of the world. A number of recent studies have made use of the recorded broadband data (e.g. Sandvol et al., 1998, Mellors *et al.*, 1997, Baker *et al.*, 1997, McNamara *et al.*, 1997, Rodgers *et al.*, 1997, Mokhtar *et al.*, 1997). In this paper we present maps of the average group velocity variation across the Arabian Plate. One goal of our effort was to increase the lateral resolution by incorporating as many as possible of the available wave propagation paths across the Arabian plate, and especially, incorporate observations in which the records were made within the Arabian plate. In the period range between 5 and 60 seconds we had a maximum of 916 Rayleigh and 653 Love waves. Since we relied on short paths and small events, the fewest paths are those at the longest periods where we collected 376 Rayleigh wave and 178 Love- wave observations.

1.3 Tectonic Setting

The Arabian Plate consists of two major tectonic provinces, the Arabian shield and the Arabian Platform (Figure 1). The Arabian shield covers about one third of the Arabian Peninsula and consists of Precambrian gneiss and metamorphosed sedimentary and volcanic rocks that have been intruded by granites (Powers *et al.*, 1966, Brown, 1972). The shield consists of five micro-plates (Afif, AR Rayn, Asir, Midyan, and Hijaz micro-plates (Stoeser and

Camp (1985)) which are separated by four ophiolite-bearing suture zones. These micro-plates are considered the remnants of Precambrian island arcs (Schmidt *et al.*, 1979) that accreted to form an Arabian neocraton around 630 Ma and which in turn were subjected to subsequent intra-cratonic deformation and magmatism producing the present day shield (Stoeser and Camp (1985)). Widespread Tertiary and Quaternary volcanic rocks related to initial stages of the Red Sea formation are predominant along western Arabia in the shield (Brown, 1972, Coleman, 1977).
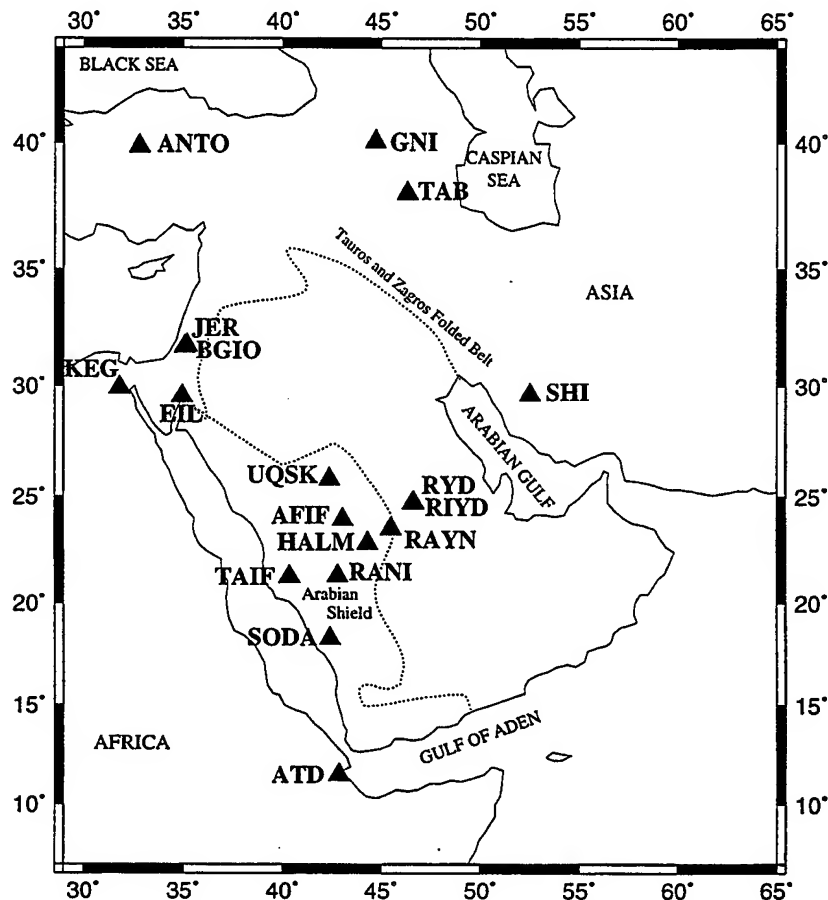
Figure 1. Tectonic provinces of the Arabian plate and the different plate boundaries.

The Arabian platform is a large sedimentary basin that comprises about two thirds of the plate and consists of Palaeozoic and Mesozoic sedimentary layers that uncomformably overlap the basement rocks and gently dip to the east (Powers *et al.*, 1966). Platform sediments increase in thickness to the east and reach a thickness of 10 km or more beneath the Mesopotamian foredeep (Brown, 1972). The western platform sediments are relatively

2

undeformed but deformation increases to the east, towards the foredeep and the Zagros and Taurus mountains. Five tectonic boundaries surround the Arabian plate (Maamoun, 1976): The continental collision boundary between the Arabian plate and the Persian and Turkish plates along the Zagros and Taurus mountains in the north and northeast; the subduction boundary in the Gulf of Oman region in southern Iran (Makran subduction zone); the transform fault boundary along the Owen Fracture zone in the southeast; the transform fault boundary along the Dead Sea fault system in the northwest; and the spreading axis along the Red Sea and Gulf of Aden in the west and southwest. All of these boundaries are tectonically active and produce an appreciable number of earthquakes, especially along the boundary associated with the Zagros mountain belt in the northeast.

1.4 Previous Geophysical Investigations

The shear-wave velocity structure of the two major tectonic provinces was modeled by Mokhtar & Al-Saeed (1994) using a surface-wave dispersion inversion. The model of the Arabian platform was found to be similar to that of East Africa and consists basically of an upper crust, 20 km thick, with shear wave velocity of 3.4 km/s overlying a 20 km thick lower crust with shear wave velocity of 4.0 km/s. Mokhtar (1995) used waveform modeling to verify the Arabian platform shear-wave velocity models of Mokhtar and Al-Saeed (1994). The Arabian shield velocity model consists of an upper and lower crust of comparable thickness to those of the platform with P-wave velocities of 6.3 km/s and 7.0 km/s for the upper and lower crust respectively (Mooney et al., 1985) and S-wave velocities of 3.6 km/s and 3.88 km/s for the upper and lower crust respectively (Mokhtar and Al-Saeed (1994)). The depth to the mantle is about 45 km beneath the platform and decreases to the southwest reaching about 40-38 km in the southwestern part of the shield (Mokhtar and Al-Saeed (1994), Mooney et al., (1985), Badri (1991)). Sandvol et al., (1998) estimated the lithospheric mantle and crustal velocity structures beneath the Arabian shield through the modeling of teleseismic P waves recorded by the temporary broadband array used in this study. Application of the receiver function techniques showed that the crustal thickness of the shield area varies from 35 to 40 km in the west adjacent to the Red Sea, to 45 km in central Arabia. These results are consistent with previous results from surface-wave inversion (Mokhtar et al., (1994), and the deep seismic refraction results (Mooney et al., (1985) and Badri (1991)). Ghalib et al., (1998) and Ghalib (1992) utilized Rayleigh-wave fundamental-mode group-velocity observations from five analog seismic stations to investigate the three-dimensional seismic structure of the Arabian plate. They reported the presence of two discontinuities at 15-22 and 35-55 km depth and the crustal velocity was found to be higher under the Arabian shield than the rest of the plate. Ritzwoller and Levshin (1998) and Ritzwoller et al., (1998) produced

tomographic maps from surface-wave group velocities across all of Eurasia. These maps were at a length scale intermediate between regional and global surface-wave studies.

Mokhtar and Al-Saeed (1994) presented two sets of dispersion data (Path II and Path III) for Love and Rayleigh-waves for the Arabian platform and one set for Rayleigh-waves for the Arabian shield (Path I). Path II extends from the eastern part of the Gulf of Aden to RYD station, while Path III connects the events in southern Iran to RYD station. There were no reliable Love-wave dispersion data for the Arabian shield reported by Mokhtar and Al-Saeed (1994). The Arabian shield has a higher group velocity than the average while the Arabian plate group velocity values are lower than the average. Similar behavior is observed for Love-waves.

1.5 Observations

We measured surface-wave group velocities generated by earthquakes located along the boundaries of the Arabian plate in the Red Sea, Gulf of Aqaba, Gulf of Aden, western Iran, Turkey, and the Dead Sea fault system. Our observations were compiled from four different sources: 1) Digital broadband seismograms from the Saudi Arabian 1995/1996 PASSCAL temporary seismic network which include about 494 seismograms from earthquakes that occurred during the period December 31, 1995 to September 15, 1996 and which represent about 50% of the Rayleigh-wave and about 60% of the Love-wave data; 2) Digital seismograms recorded by the permanent broadband stations in the region for the period between 1990 and 1996 which represent 26% of the Rayleigh-wave and 36% of the Love-wave data; 3) Analog observations of Rayleigh waves from the regional WWSSN stations recorded between 1970 and 1979 which represent 19% of the total Rayleigh-wave data; and 4) Analog observations from RYD station recorded between 1981 and 1987 which represent 5% of both Rayleigh- and Love-wave data.

In Figures 2 and 3 we present the great circle path coverage along which dispersion measurements were made for both Love- and Rayleigh-waves. A total of 987 Rayleigh-wave and 682 Love-wave paths were available. A maximum of 916 rays for Rayleigh and 682 rays for Love were used in the period range of 11-13 seconds (this is the average of the total number of ray paths over the 3 periods). The number of great circle paths decreases for longer periods and reaches 376 for Rayleigh and 178 for Love at 56-60 s periods. Seismic stations used in this study are also shown in these Figures and include the XI95-96 IRIS PASSCAL digital broadband stations AFIF, HALM, RAYN, RIYD, RANI, TAIF, UQSK, and SODA; regional broadband GSN seismic stations ANTO, GNI, BGIO, KEG, and ATD; and the WWSSN stations from which analog data were digitized (TAB, SHI, EIL, JER, and RYD).

4
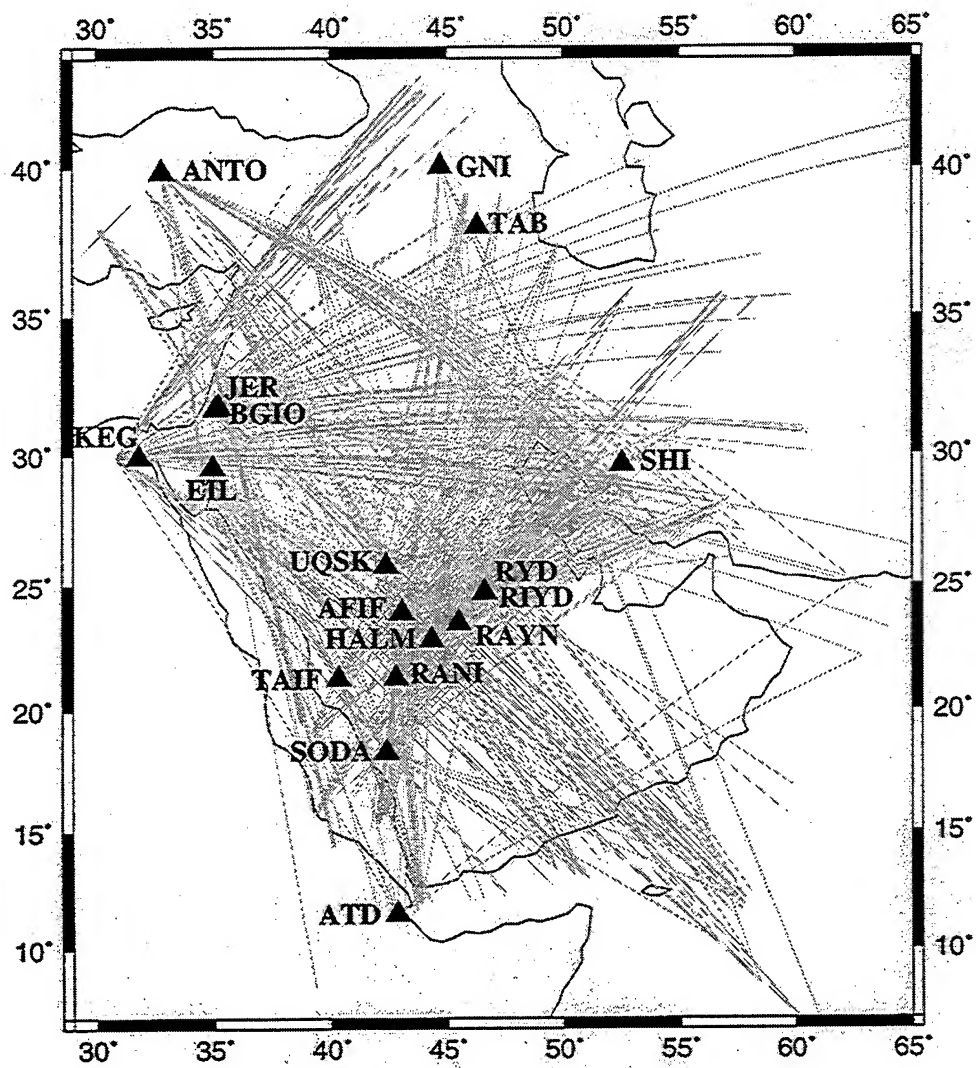
Figure 2. Distribution of ray path coverage for Love-waves.
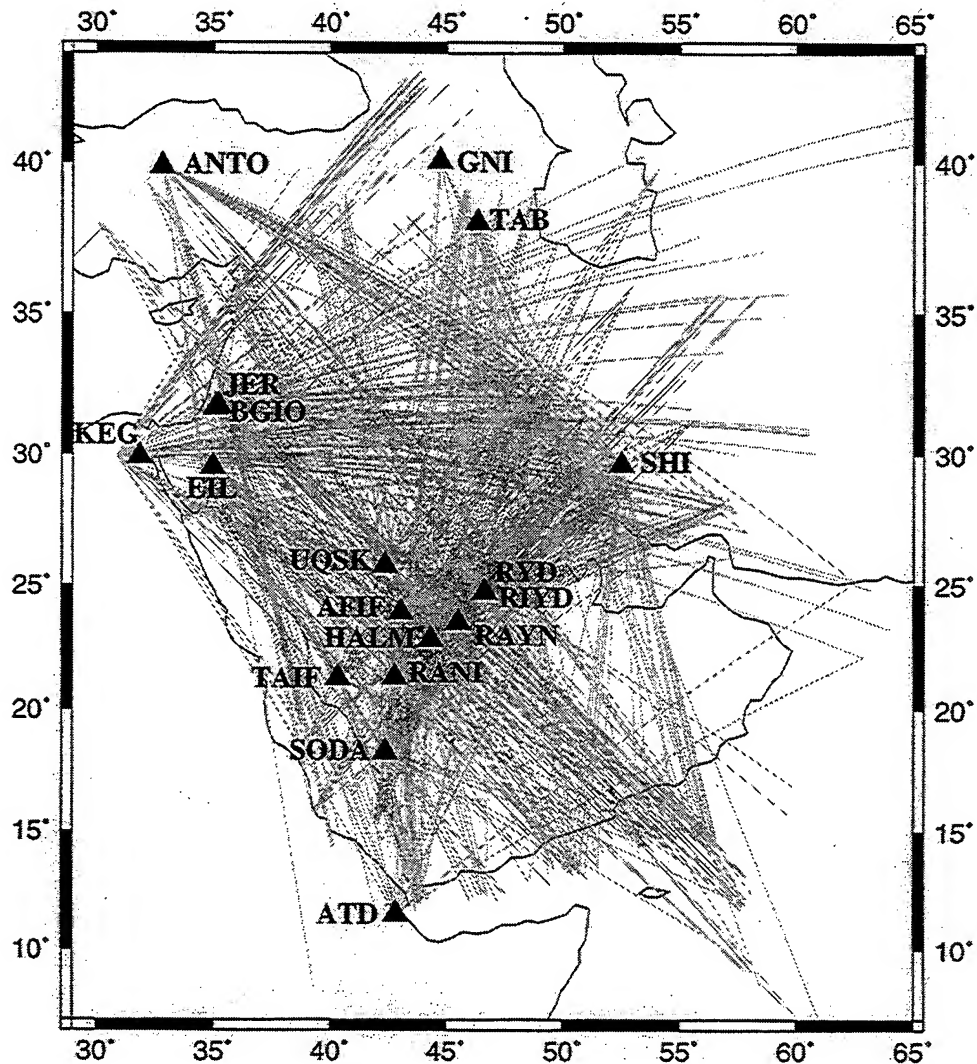
Figure 3. Distribution of ray path coverage for Rayleigh waves.

The regional-scale tomographic maps presented below provide significant constraints on the shear velocity and crustal thickness of the Arabian plate. These data were recorded mainly by seismic stations inside the plate or very close to its tectonic boundaries, and avoiding long paths that may traverse a number of different tectonic provinces and geological features. Surface waves propagating at regional distances are very useful in the period range of interest in this study by contributing shorter periods and increased resolution. The stations deployed in Saudi Arabia provided significant coverage of the

Arabian shield. The data set also has significant coverage of the western part of Iran and all of Iraq.

1.6 Methods of Analysis

We present the results of regional tomographic inversion of dispersion data from Rayleigh and Love waves across Arabia using single station measurements of group velocity and applying the multiple filtering analysis technique (Dziewonski *et al.*, 1972, Herrmann, 1987).

The dispersion measurements are obtained at period increments of 1 second between 5 and 20 seconds and at even periods only in the range 22-60 seconds. Observations from each period are inverted separately and the images from adjacent periods were averaged. We parameterize the regional slowness variations using a uniform, one-degree by one-degree, grid of constant-slowness cells. Group velocity maps are produced using a conjugate-gradient least squares algorithm (Paige and Sanders, 1982). Laplacian smoothness constraints are incorporated in the inversion and thus we minimize a combination of group travel time misfit and a Laplacian measure of a two dimensional model roughness. The balance between group delay misfit and minimal roughness is selected empirically by running inversions with a range of smoothness importance weights and selecting the value that produces the simplest model and still satisfactorily matches the observed group delays. The resulting velocity variations are presented as percent velocity perturbations from the average velocity of all the measurements (which was the initial model).

We assume that the measured waves have propagated along the great circle path connecting the source and the receiver. Ritzwoller and Levshin (1998) discussed the problems expected to result from several factors such as off-great circle propagation, azimuthal anisotropy, and systematic event mislocations near subducting slabs, and argued that these effects should not alter the tomographic maps of group velocities strongly beyond the resolution estimates. In addition, our use of short- distance paths helps minimize the likely deflection of the path from the great-circle arc.

1.7 Resolution

Estimating the resolution in a tomographic inversion is not a trivial task because resolution depends on complex factors such as the number of crossing rays, the density of sources and receivers, as well as random and possible systematic uncertainty in the measurements. To estimate our resolving capability, we used standard "checker-board" tests. Specifically, we tested two models. Each of the two models consists of 1° x 1° cells in which a velocity perturbation of +- 10% of the average was chosen to have a dimension of 3° x 3° for the first model and 8° x 8° for the second model (Figure 4). The checker-board test results show that features of dimension 8° x 8° are reasonably recovered, especially in the short period ranges where the number of ray

paths is maximum. In contrast, features of dimensions smaller than that are hardly recognized using the current coverage of the data available. The precise amplitude of the anomaly is difficult to estimate due to dependence on damping and smoothing (which complicates tests involving models with sharp contrasts) but the pattern of variations is reasonably well reconstructed. We performed tests for both Love and Rayleigh waves and tested the resolution for the maximum and minimum number of ray paths in each case.
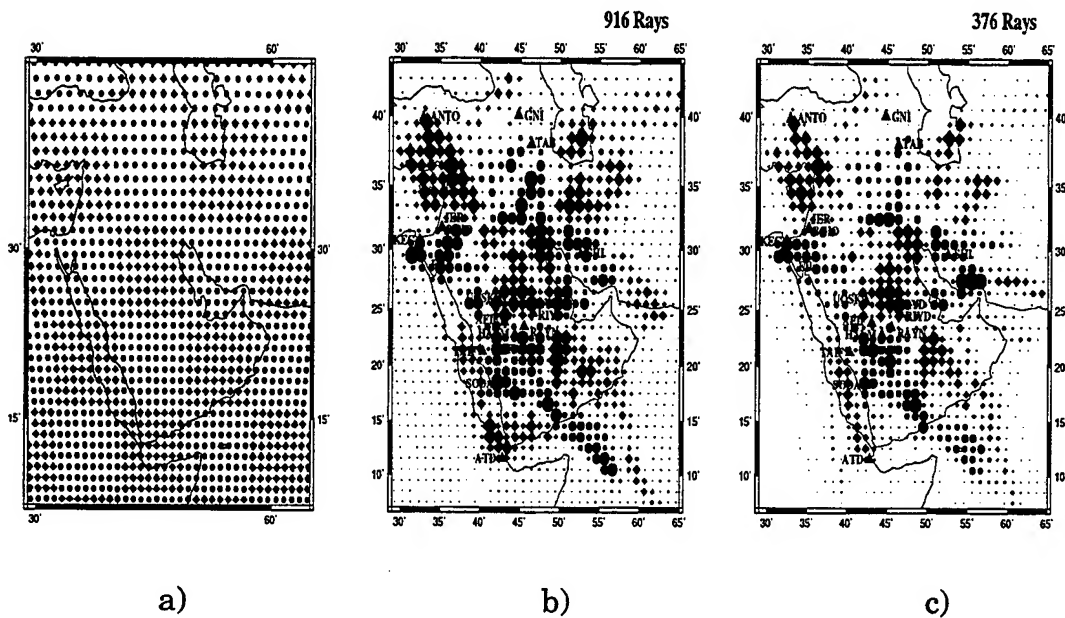
Figure 4. Checker board test results: a) The original velocity perturbation model using a feature of 8° x 8° in dimension. b) Tomographic inversion results for Rayleigh-waves using the maximum number of rays. c) Rayleigh-waves results using the minimum number of rays.

1.8 Group Velocity Variations in the Middle East

In Figure 5 and Figure 6 we present the tomographic images constructed for Love and Rayleigh waves respectively. Each map shows the average group velocity variations for three adjacent periods and above each map we list the average group velocity for that period range and the average number of rays for the same periods. One striking observation in these maps is the consistency of the results from both Rayleigh and Love waves. The distribution of faster and slower than average regions is strikingly similar in both data sets, especially in the short periods. It is clearly evident that the Arabian shield is characterized by relatively higher than average seismic velocity, while the rest the Arabian platform, which is covered by an eastward-

thickening sedimentary section, has in general slower than average velocity. The boundary between the fast and slow regions is sharp and correlates well with the boundaries of the Arabian shield, especially at periods shorter than 10 seconds. For longer periods, a fast region correlates well with the boundaries of the Red Sea, especially for the Rayleigh waves. In general, the seismic velocity is higher in western Arabia than in the eastern or the northeastern parts of the plate. The resolution diminishes for long periods where the number of rays becomes smaller. The average group velocity of Love waves increases from about 2.44 km/s at 5-7 seconds to 3.98 km/s at 56-60 seconds, while that of Rayleigh waves increases from 2.38 km/s at 5-7 seconds to 3.74 km/s at 56-60 seconds. The mean velocities at our longer periods (50-60 s) are about 8% slow for Love waves, but only about 3% slow for Rayleigh waves.

We do not have adequate coverage to image the southeastern part of the Arabian plate where it is covered mainly by the Empty Quarter region and the localized fast anomaly located east of the Gulf of Aden. The slow feature located in the eastern Mediterranean region should be interpreted as a result of bias in the data since there are not enough traverses crossing this region. The resolution of the oceanic structure south of the Arabian plate is limited to a small region that produces an apparent localized heterogeneity. Our results are consistent with those of Ghalib (1992) who analyzed analog seismograms recorded at stations TAB, SHI, EIL, and JER to outline the lateral variation of shear-wave velocity beneath the Arabian plate for depths from 5 to 80 km. Ghalib (1992) concluded that shear wave velocity within the crust is higher in the shield region than in the platform area for depths less than 40 km, but the pattern is reversed at depths below 40 km. This is consistent with the conclusion of Woodhouse and Dziewonski (1984) regarding the possible existence of low-velocity anomalies in the upper mantle along the western and southwestern Arabian plate.
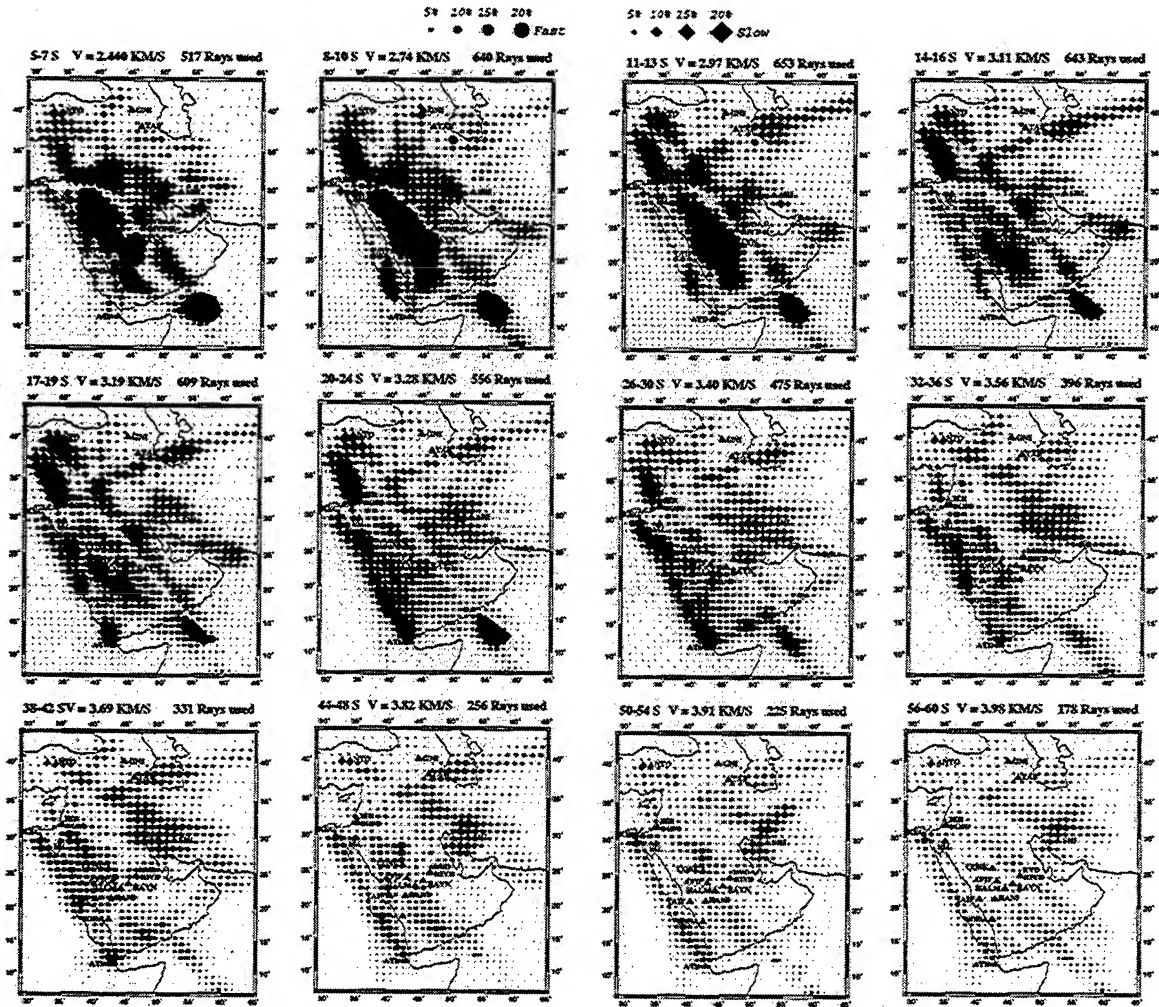
Figure 5. Tomography map of the Arabian plate Love-wave group velocity. The legend shows the % of the velocity perturbations. The average group velocity and the average number of rays used are given for each period interval.
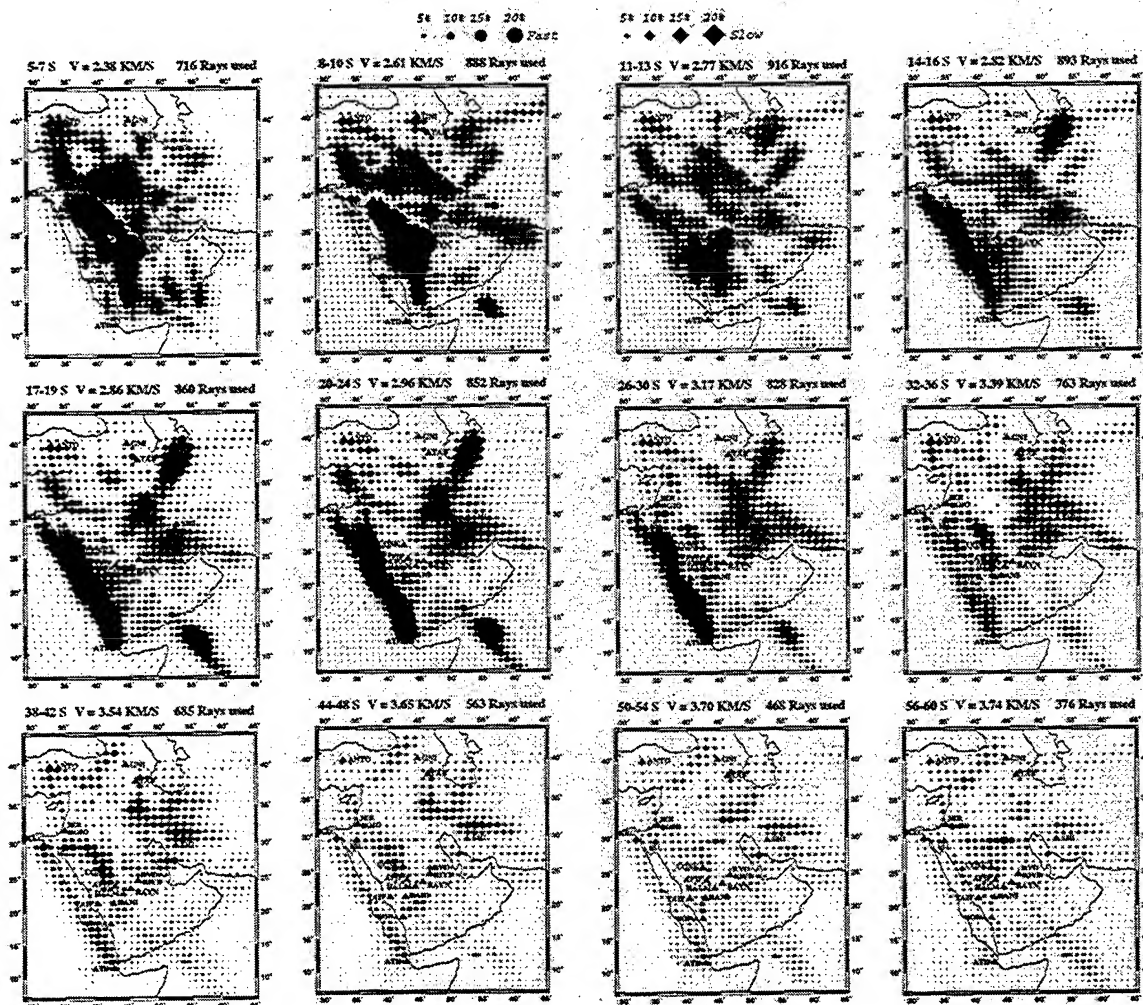
Figure 6. Tomography map of the Arabian plate Rayleigh-wave group velocity.

1.9 References

Badri, M., (1991). Crustal structure of central Saudi Arabia determined from seismic refraction profiling. *Tectonophysics,* **185,** 357-374.

Baker, G. E., T. G. Barker, and K. L. McLaughlin (1997). Sources and propagation effects on regional phase amplitudes in the Middle East (Abstract). *American Geophysical Union Fall Meeting,* **78,** No. 46, F428.

Brown, G. F., 1972. Tectonic map of the Arabian Peninsula, Saudi Arabian Peninsula Map AP-2. *Saudi Arabian Dir. Gen. Miner. Resour.*

Coleman, R. G., 1977. Ophiolites. Ancient Oceanic Lithosphere? *Springer-Verlag,* Berlin, 229 pp.

Dziewonski, A. M. and Hales, A. L., 1972. Numerical Analysis of dispersed seismic waves. In: B. Alder, S. Frenbach and M. Rotenberg (Editors), *Methods in Computational Physics.* Academic Press, New York, NY, pp. 39-85.

Ghalib, H. A. A., 1992. Seismic velocity structure and attenuation of the

Arabian plate, *Thesis, Saint Louis University, Saint Louis, Missouri, USA*, 350 pp.

Ghalib, H. A. A., T. A. Mokhtar, and R. B. Herrmann (1998). Variation of the seismic velocity structure of the Arabian plate, PL-TR-97-2301, *Phillips Laboratory, Hanscom AFB, MA.*

Herrmann, R. B. (Editor), 1987. *Computer Programs in Seismology, VOL I-VOL VII.* Saint Louis University, Saint Louis, Missouri, USA.

Maamoun, M., 1976. La seismicite du Moyen et du Proche-Orient dans le cadre de la seismotectonique mondiale. *These, Doc. Sci.*, Univ. Louis Pasteur, Strasbourg.

McNamara, D. E., S. E. Hazler, and W. R. Walter (1997). Velocity structures across northern Africa, southern Europe, the Middle East and the Arabian Peninsula from surface wave dispersion (Abstract). *American Geophyiscal Union Fall Meeting,* **78, No. 46,** F499.

Mellors, R. J., F. Vernon, A. M. Al-Amri (1997). Characterization of Regional Waveform propagation in the Saudi Arabian Peninsula by Waveform stacking (Abstract). *American Geophyiscal Union Fall Meeting,* **78,** No. 46, F428.

Mokhtar, T. A., C. J. Ammon, H. A. A. Ghalib, and R. B. Herrmann (1997). Lithospheric structures beneath Arabia (Abstarct). *American Geophyiscal Union Fall Meeting,* **78,** No. 46, F499.

Mokhtar, T. A., and M. M. Al-Saeed (1994). Shear wave velocity structures of the Arabian Peninsula, *Tectonophysics,* **230:** 105-125.

Mokhtar, T. A. (1995). Phase velocity of the Arabian Platform and the surface waves attenuation characteristics by wave from modeling, *Jour. King Abdulaziz Univ., Earth Sci.,* **8,** 23-45.

Mooney, W. D., M. E. Gettings, H. R. Blank, and J. H. Healy (1985). Saudi Arabian seismic deep- refraction profile: a travel time interpretation of crustal and upper mantle structure. *Tectonophysics,* **111,** 173-246.

Paige, C. C., and M. A. Saunders, LSQR: An algorithm for sparse linear equations and sparse least squares, *ACM Trans. Math. Softw.,* **8,** 43-71, 1982.

Powers, R. W., L. F. Ramirez, C. P. Redmond, and E. L. Elberg, 1966. Geology of the Arabian Peninsula-sedimentary geology of Saudi Arabia. *U. S. Geol. Surv. Prof. Pap.* **560-D,** 147 pp.

Ritzwoller, M. H., and A. L. Levshin (1998). Eurasian surface wave tomography: Group velocities, in press.

Ritzwoller, M, H., and A. L. Levshin (1998). Intermediate period group velocity maps across central Asia, western China, and parts of the Middle East, in press.

Rodgers, A., and W. Walter (1997). Lithospheric structure of the Middle East from complete waveform modeling (Abstract). *American Geophyiscal Union Fall Meeting,* **78,** No. 46, F495.

Sandvol, E., D. Seber, M. Barazangi, F. Vernon, R. Mellors, and A. Al-Amri

(1998). Lithospheric velocity discontinuities beneath the Arabian shield, in press.

Schmidt, D. L., D. G. Hadley, and D. B. Stoeser (1979) Late Proterozoic crustal history of the Arabian shield, southern Najd province, Kingdom of Saudi Arabia, evolution and mineralization of the Arabian-Nubian shield. *I. A. G. Bull.,* **3 (2)** 41-58.

Stoeser, D. B., and V. E. Camp, 1985. Pan-African microplate accretion of the Arabian shield. *Bull Geol. Soc. Am.,* **96,** 817-826.

Vernon, F, and J. Berger (1997). Broadband seismic characterization of the Arabian shield, *Interim scientific and technical report,* 17 pp.

Woodhouse, J. H., and A. M. Dziewonski (1984). Mapping the upper mantle: Three-dimensional Modeling of the earth structure by inversion of seismic waveforms, *J. Geophys. Res.,* **89,** 5953-5986.

2. CRITERIA FOR USING GENETIC ALGORITHM TO MODEL SUR-FACE-WAVE WAVEFORMS

Tao-Ming Chang, Robert B. Herrmann, and Charles J. Ammon

2.1 Abstract

In this study, we evaluate the suitability of four criteria in modeling complicated waveforms such as surface waves. We design these four criteria using some direct measurable quantities such as N1, N2 norm, normalized cross-correlation value at zero time lag, and time shift information of maximum envelope and maximum amplitude of cross-correlation. The tests are performed using a genetic algorithm search method. Seventeen repeated experiments are conducted. Each experiment has four GA runs with different criteria. The test results suggest that the criterion that combines phase and group velocity information is the best for modeling surface-wave waveforms. The result of one randomly chosen experiment is shown and an oversimplified case is used to explain why this criterion is better than the others.

2.2 Introduction

Among seismological applications, the most common criterion of goodness-of-fit is the L2 norm. This is because most seismological optimization problems are implemented using least squares minimization. For discrete data points, the least squares method and L2 norm are the natural choice. Indeed, for most studies the L2 norm behaves well and the resulting surface-wave dispersion data inversion, modeling of teleseismic P waveforms, or receiver function inversion is acceptable. There is no need to further investigate the other possible criteria.

Some people feel it is not totally convincing to use this simple criterion for every problem, especially when they try to use an L2 norm to model somewhat complicated waveforms; for these cases they are starting to use more complicated criteria. For example, Zhu and Helmberger (1996) modified Zhao and Helmberger's method (1994) to extract source information from broadband regional seismograms by using combined L1 and L2 norms. Other norms have been used to model the surface-wave waveforms. Lerner-Lam and Jordan (1983) and Cara and Leveque (1987) used cross-correlation techniques to formulate inversion schemes for inverting surface-wave waveforms. Therefore, we feel that the success of the simple L2 norm may be due to the simplicity of the problems, such as the use of travel times in determining hypocenter locations, teleseismic P waveforms in estimating source parameters, or receiver functions in inverting velocity structures underlying receiver sites.

However, we believe there is a need to use complete waveforms to extract more information in order to better constrain earthquake source processes and propagation effects. Hence it is time to examine the suitability of

different criteria for the inverse problems.

2.3 Purpose

In this study, we will use the genetic algorithm (hereafter GA) as a tool to check the suitability of several criteria. It is not practical to test many criteria on different types of seismic signals, so we limit ourselves to modeling surface-wave waveforms. The test results will be useful only for this application.

2.4 Basic Components For Designing Criteria of Goodness-of-Fit

In implementing the GA search method, we note that the goodness-of-fit criterion is user defined, and can be a combination of a variety of different criteria. The design of a goodness-of-fit criterion for modeling a surface wave is very subjective and depends on the features of the surface-wave signal itself. To begin with the design of the criterion, it is necessary to understand the characteristics of the object which will be modeled.

There are two major characteristics of surface waves. First, a surface-wave signal has a longer duration and a more complicated waveform than any single, pulse-like body-wave phase. When modeling such long-duration complicated waveforms, there is a cycle-skipping problem which may produce an unreasonably low or high velocity model. In addition, when processing surface-wave data, we cannot shift synthetic seismograms to match the observed arrival time, a well adopted technique in processing body wave data in the case of a receiver function inversion. Therefore, the cycle-skipping problem will be the first problem that will need to be resolved. Second, surface waves usually have a broad frequency content. Any single measurement from a waveform may not be adequate to represent the whole waveform because of the variability in amplitude levels as a function of frequency. For example, a single cross-correlation measurement only represents the similarity of the shape of the largest amplitudes, which are typically high-frequency for shallow crustal earthquakes in broadband data. This will only resolve the very shallow part of the structure and will leave the deeper structure uncertain with high variation. To overcome this problem, we can divide the frequency range of interest into several subranges and evaluate the goodness-of-fit of narrow-band filtered observed and synthetic seismograms for each subrange. For our tests on regional seismograms, we divided the period range (10-50 sec) into 4 intervals : (10-20 sec), (20-30 sec), (30-40 sec), (40-50 sec). Using these period intervals as the ranges to bandpass filter observed and synthetic seismograms, a cross-correlation value is computed for each interval and a composite cross-correlation can be used as our goodness-of-fit.

In this study, several different criteria have been tested as indicators of goodness-of-fit. Some of them are direct measurements from waveforms, the rest of them are a combination of those direct measurements. The direct measurements include the N1 norm ($N1$), N2 norm ($N2$), normalized cross-

correlation value at zero time lag (CC_0), the time shift of envelope of cross-correlation (TS_u), and the time shift of maximum cross-correlation (TS_c) of windowed narrow-band filtered observed and synthetic seismograms. These basic criteria are briefly described.

2.4.1 N1 Norm (N1)

For each sub-period range, the N1 norm is constructed from a normalized L1 norm as

$$V_j = \frac{\sum W(t_i) \cdot |F_j * obs(t_i) - F_j * syn(t_i)|}{\sum W(t_i) \cdot |F_j * obs(t_i)|} \tag{1}$$

where $W(t_i)$ is a cosine taper window which approximately has corners corresponding to group velocities of 4.8 and 2.6 km/sec, F_j is a band-pass filter, * means convolution, and $obs(t_i)$ and $syn(t_i)$ represent observed and synthetic seismograms respectively at time t_i. The value from above equation will range from zero to some positive number. However in our GA search, the goodness-of-fit value is mapped into the range [0.0 , 1.0]. It is also necessary to map the V_j value into 1.0-0.0 range. The mapping procedure used in this study is as follows

$$N1_j = \begin{cases} 1 - \log_{10}(1 + V_j) \cdot 1.5 & 0 \le V_j \le 3.64158 \\ 10^{-6} & V_j > 3.64158 \end{cases} \tag{2}$$

Of course, the measurement can be performed for several wide-band frequencies (using a Butterworth filter) or several narrow-band frequencies (using a Gaussian filter). The goodness-of-fit value N1 is actually the combination of different frequency bands which emphasizes a solution that fits all frequency bands well. In the following, we use a geometric instead of arithmetic mean for goodness values of different frequency bands.

$$N1 = \left[\prod_{j=1}^{n} N1_j(f_j) \right]^{\frac{1}{n}} \tag{3}$$

In a more complete form, the N1 norm used is

$$N1 = \left\{ \prod_{j=1}^{n} \left[1 - \log_{10} \left(1 + \frac{\sum W(t_i) \cdot |F_j * obs(t_i) - F_j * syn(t_i)|}{\sum W(t_i) \cdot |F_j * obs(t_i)|} \right) \cdot 1.5 \right] \right\}^{\frac{1}{n}} \tag{4}$$

2.4.2 N2 Norm (N2)

Using the same mapping procedure as for the N1 norm, the N2 based norm is defined as

$$N2 = \left\{ \prod_{j=1}^{n} \left[1 - \log_{10} \left(1 + \frac{\sum W(t_i) \cdot (F_j * obs(t_i) - F_j * syn(t_i))^2}{\sum W(t_i) \cdot (F_j * obs(t_i))^2} \right) \cdot 1.5 \right] \right\}^{\frac{1}{n}} \quad (5)$$

Like our N1 norm, this norm equally weights different sub-frequency bands instead of the dominant frequency band, but internally uses an L2 norm.

2.4.3 The Cross-Correlation Value at Zero Time Lag (CC_0)

To model a surface-wave waveform, we hope that for every frequency range the normalized cross-correlation value at zero time lag equals unity, which means the synthetic seismogram is perfectly aligned with the observed seismogram. The normalized cross-correlation value ranges from -1 to 1. The following mapping procedure will emphasize the in-phase part.

$$CC_0 = \left(\frac{1 + \Phi(0)}{2} \right)^2 \quad (6)$$

where $\Phi = [W(t_i)F_j * obs(t_i)] \otimes [W(t_i)F_j * syn(t_i)]$ is the normalized cross-correlation of windowed narrow-band filtered observed and synthetic seismograms.

2.4.4 The Time Shift of Maximum Envelope Value of Cross-Correlation (TS_u)

The physical meaning of the time shift of the maximum envelope value of the cross-correlation of windowed narrow-band filtered observed and synthetic seismograms can be closely related to the difference of group velocity between observed and synthetic seismograms at that particular frequency. For modeling a surface-wave waveform, the best solution is that for all frequency subintervals there are no time shifts between observed and synthetic seismograms. The time shift (TS_{u_j}) for each sub-period interval is measured from the maximum envelope value of the cross-correlation away from the zero time lag. The averaged absolute time shift will range from zero to some positive number. Here another mapping procedure, different from the N2 norm mapping procedure, is needed to map time shift information into the goodness range $(0, 1)$. The mapping procedure will be as follows: Assume surface waves travel with a group velocity of about 3.5 km/sec. First compute the percentage of time-shift with respect to the total travel time. Then, map it into the goodness range $(0, 1)$ using the following equation:

$$TS_u = \left[\prod_{j=1}^{n} \left(\frac{1}{1 + \frac{|TS_{u_j}|}{dist/3.5}} \right)^{10} \right]^{\frac{1}{n}} \quad (7)$$

This criterion guarantees that for each subinterval the goodness value will be

equal to one when there is no time shift and the goodness will be 0.5 when the travel time difference reaches roughly 7%. The function TS_u penalizes a poor fit.

2.4.5 The Time Shift of Maximum Value of Cross-Correlation (TS_c)

This criterion is closely related to phase velocity. Similar to TS_u, when modeling a surface wave, we wish this time shift to be zero. The time shift is measured from the maximum value of the cross-correlation with respect to zero time lag. Using the same mapping procedure as TS_u, the TS_c is defined by the following equation.

$$TS_c = \left[\prod_{j=1}^{n} \left(\frac{1}{1 + \frac{|TS_{c_j}|}{dist/3.5}} \right)^{10} \right]^{\frac{1}{n}} \tag{8}$$

2.5 Four Combined Criteria

Having defined several functionals that characterize a fit, we now create some combinations for testing overall fit.

2.5.1 Criteria 1

The first criterion which will be tested is (9). The concept behind the design of this criterion is that we want the GA search to focus on the models that minimize both L1 and L2 based norms for every sub-frequency band. Initially, the N2 norm will be strongly affected by the biggest amplitude signal, but the N1 norm will be less influenced by the largest amplitudes and will permit the small amplitude seismic signals to play a slightly more important role.

$$\{N1 \cdot N2\}^{\frac{1}{2}} \tag{9}$$

2.5.2 Criteria 2

The second criterion is given by (10). It is well-known that using a single type of surface-wave dispersion data (such as group velocity or phase velocity) in an inversion will not necessarily match the waveform. This is because the inverted model which matches group velocity data may have a phase change, and results that match phase velocity data may still have a group delay. This is why we combined both types of information in this criterion. We hope the GA search will find models that have no time shifts in group and phase velocity for every sub-frequency interval.

$$\left\{ TS_u \cdot TS_c \right\}^{\frac{1}{2}} \tag{10}$$

2.5.3 Criteria 3

The third criterion is (11). This criterion is similar to the second criterion but has a CC_0 term. The CC_0 contains redundant information because when a model has no time shift between observed and synthetic seismograms, the normalized cross-correlation value at zero time lag will be unity. The design of this criterion is for a comparison with Criteria 2 to see whether extra information will help the search converge faster.

$$\left\{ CC_0 \cdot \left[TS_u \cdot TS_c \right]^{\frac{1}{2}} \right\}^{\frac{1}{2}} \tag{11}$$

2.5.4 Criteria 4

The last criterion is (12). This is a combination of Criteria 1 and 3. We wish to consider the performance when a criterion utilizes all the possible information.

$$\left\{ [N1 \cdot N2]^{\frac{1}{2}} \cdot \left[CC_0 \cdot (TS_u \cdot TS_c)^{\frac{1}{2}} \right]^{\frac{1}{2}} \right\}^{\frac{1}{2}} \tag{12}$$

The criteria constructed have as their goals a characterization of a good visual effect and a sensitivity to sharply reject models that do not provide a good fit.

2.6 Test Results

It is impossible to reach a definitive conclusion based on one experiment. We use these four criteria in a GA search. We repeated this testing procedure for 17 experiments with small variations in the starting model. The number of experiments may not form a significant base from a statistical viewpoint, but we reach some understanding about the capabilities of different criteria. In the following section, we randomly choose one experiment result as an example to show the search results.

The experiment has four GA search tests which use the different criteria. For each search test, we will show groups of three figures. The first figure in a test will show the ten best models, their waveform comparisons with the observed seismogram (filtered between 10 and 100 seconds and displayed from 50 to 250 seconds), and the distribution of searched models with goodness values greater than a certain threshold. The second figure will show the seismograms of the ten best final models filtered in 4 period-ranges, (10-20 sec), (20-30 sec), (30-40 sec), and (40-60 sec), displayed in a 100 to 300 second travel-time window together with the observed seismogram. The third figure

consists of two parts. The first part shows the group velocity extracted from observed and synthetic seismograms of the ten best final models using the multiple filter technique (Dziewonski *et al.,* 1969; Herrmann, 1973). The second part shows the averaged velocities of the top 30, 40, 60, and 80 km of all searched models with respect to goodness-of-fit values.

The first GA search test used the Criteria 1. The results are shown in Figures 7, 8, and 9. In Figure 7, we can see the peak amplitude of the seismogram of the best model is time aligned better than the sixth best model. However from Figure 8, we can see that the first model does better in the 20-30 second range and that this is the reason why the first model has a higher goodness value than the sixth model. Figure 9 shows two empirical ways to present the uncertainty of searched models. The group velocity curve can indicate the period range that deviates most from the observed curve. The shear velocities averaged over the upper 30, 40, 60, and 80 km show whether the GA searched models converge to a value which can be used to reconstruct the velocity profile.

The second GA search test used the Criteria 2. The results are shown in Figures 10, 11, and 12. The synthetic seismogram of the best searched model fits the observed waveform very well with only a slightly slow higher mode. In Figure 12, we see that these ten models have their group velocity curves within ± 0.1 km/sec range of the observed curve. However, for periods less than 10 seconds, none of the ten best models match the very low group velocity. That can be explained because the "observed" model has a very low velocity sediment layer at the top which may produce this very low group velocity for periods less than 10 seconds, which is beyond our modeling range.

The third GA search test used the Criteria 3. The results are shown in Figures 13, 14, and 15.

The last GA search test used Criteria 4, with results shown in Figures 16 - 18.

Although all these criteria can find models that fit the waveform reasonably well, we need a way to compare the effectiveness of the models resulting from these four different criteria. Note that goodness-of-fit values the from different criteria are not directly comparable. To properly compare, we use the best model from each GA search test and evaluate it against each of the four criteria. The results are listed in Table 1. To understand this table, we would expect a criteria to give the best possible model, so that the diagonal would be dominant. In Table 1, the four evolutions of the best model of each GA search test are placed in one column. For a given model, the values of the other Criteria fill in the row. Table 1 indicates that the Criteria 3 model (row 3) has the best value under TEST 2, 3 and 4 and is marginally poorer under TEST 1 than the model for Criteria 2 (2nd row).
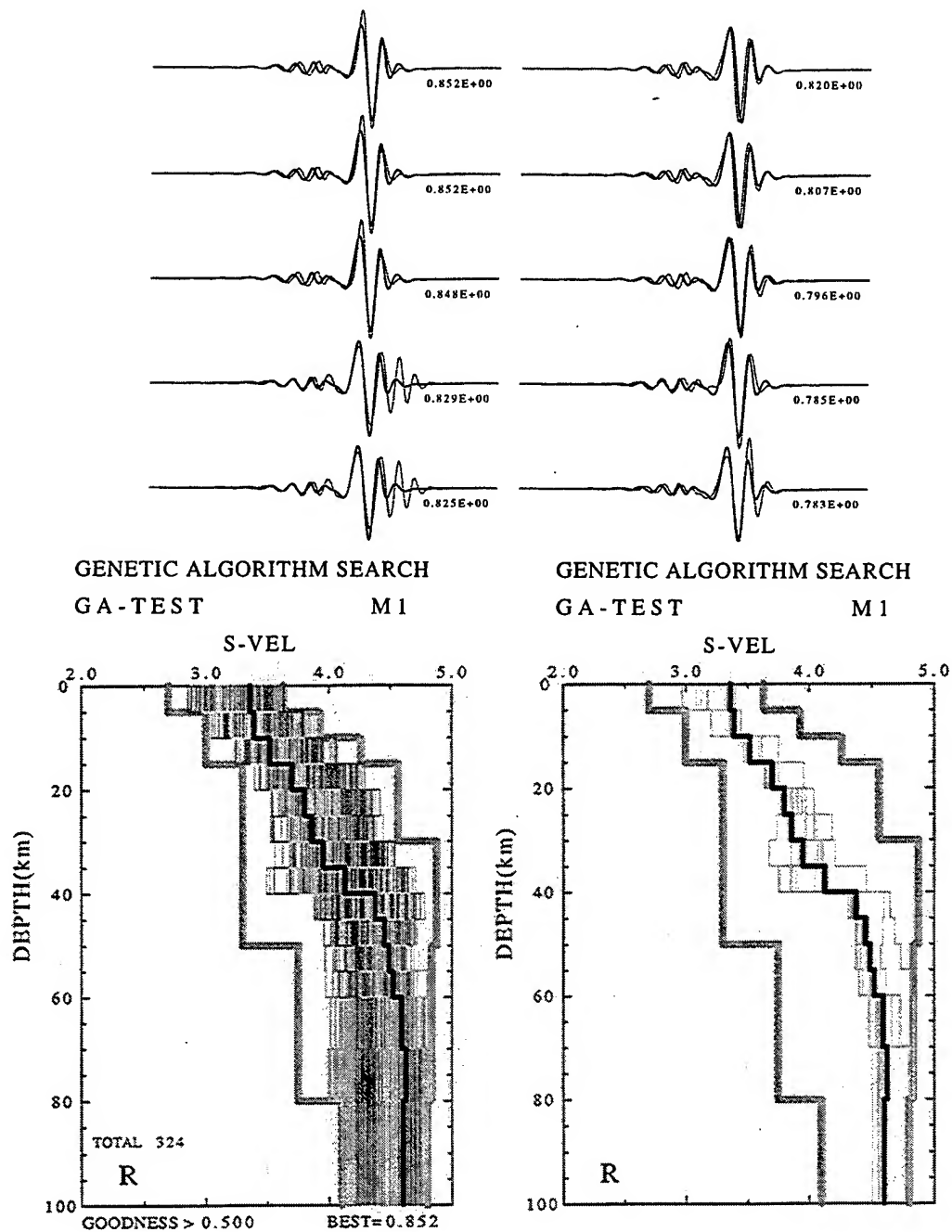
Figure 7. The GA search results using Criteria 1. The waveforms of ten final best searched models (gray) are compared with the observed waveform (black). The displayed seismograms are filtered between 10 and 100 seconds, and the displayed range is 50 to 250 seconds. The right bottom plot shows these ten models and the best one is plotted as a heavy black line. The left bottom plot shows searched models with goodness values greater than 0.5. Lighter shades of gray imply a better fit. The outer bounds of the search are also indicated.
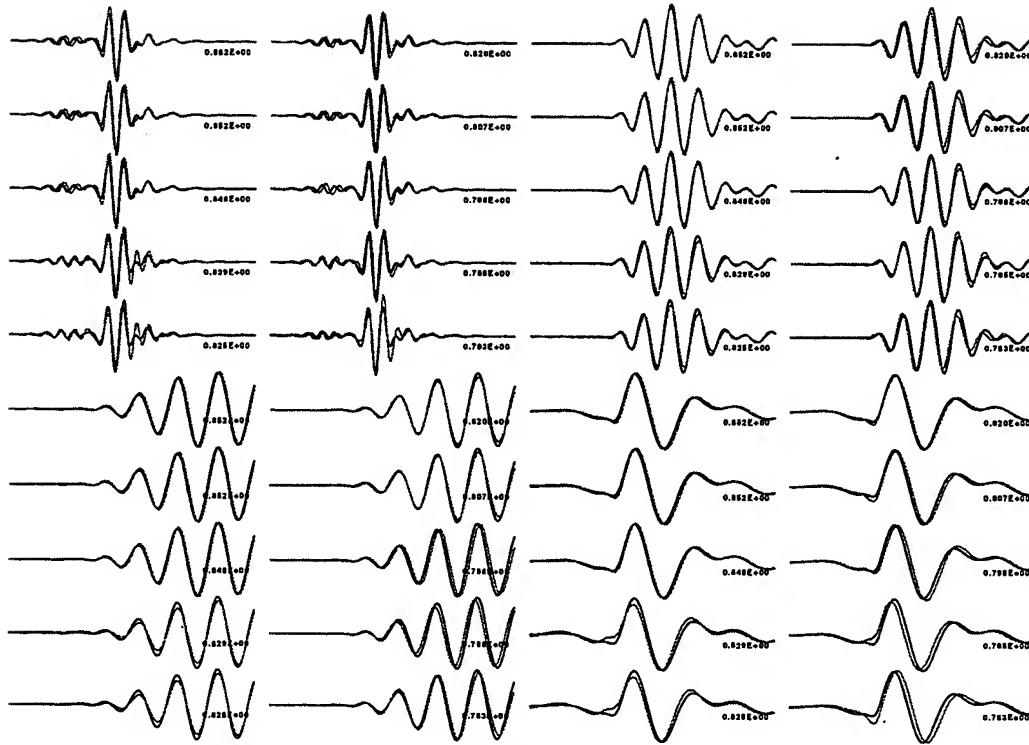
Figure 8. The observed and synthetic seismograms of ten models have been filtered in four different period ranges. The top left part is filtered for 10 to 20 seconds. The top right part is filtered for 20 to 30 seconds. The bottom left part is filtered for 30 to 40 seconds. The bottom right part is filtered for 40 to 60 seconds. The seismograms are displayed for 100 to 300 seconds.

Table 1. The goodness values for 4 GA search tests

Model from	TEST 1 (Criteria 1)	TEST 2 (Criteria 2)	TEST 3 (Criteria 3)	TEST 4 (Criteria 4)
Criteria 1	**0.851907**	0.873815	0.899356	0.860601
Criteria 2	0.974151	**0.961544**	0.978459	0.945162
Criteria 3	0.972166	0.971157	**0.981818**	0.953598
Criteria 4	0.910052	0.921201	0.939683	**0.905907**

To compare the abilities of criteria we introduce two voting schemes. In the first, we examine each row to seek the biggest value for that criteria and give a vote to that GA Search test. In the second, we check the diagonal values to see whether its value is the largest in that row. If answer is yes, we give a vote to that GA search test at that column. For example, from Table 1, TEST
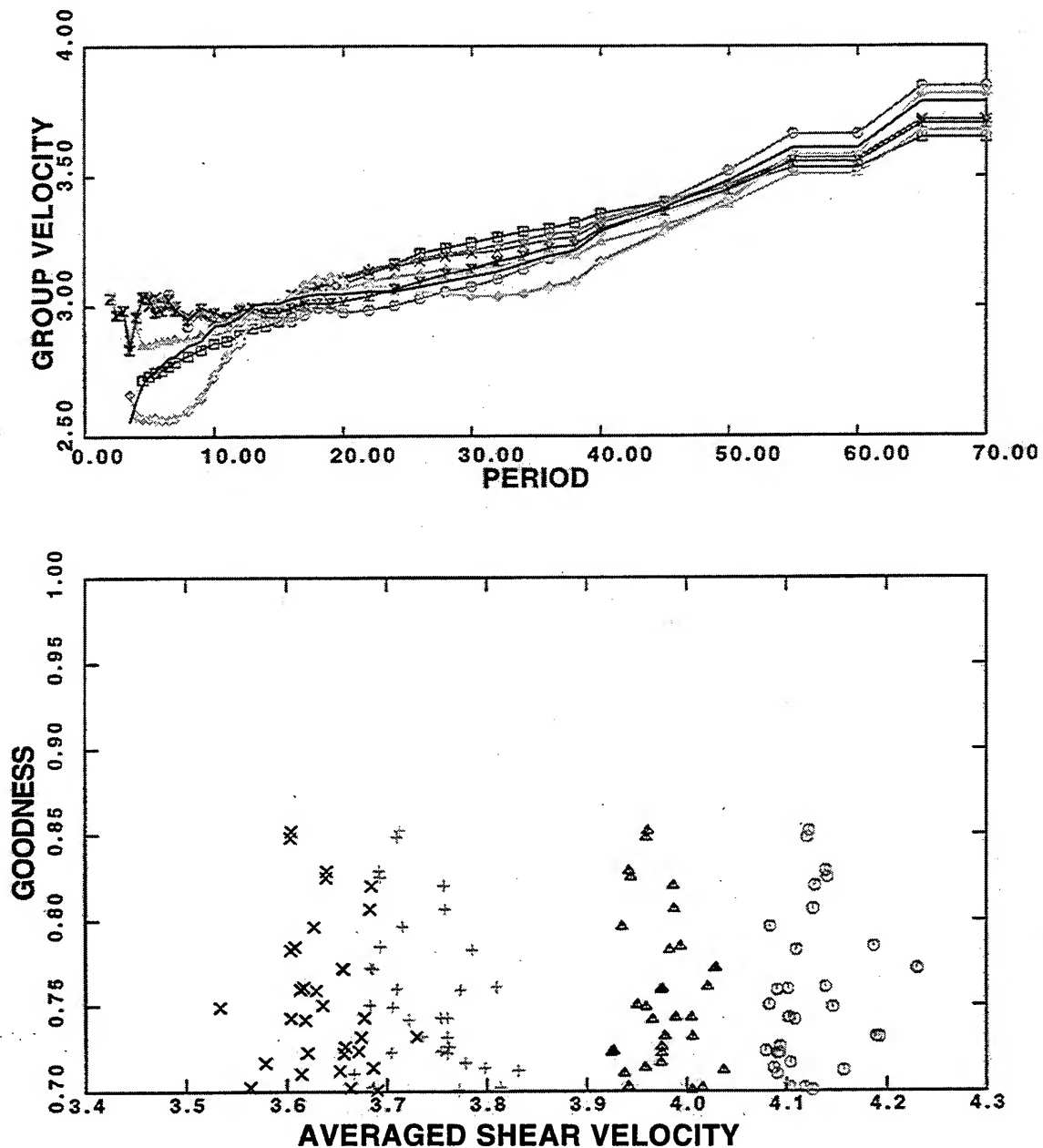
Figure 9. The top panel shows the group velocity (km/sec) information extracted using the MFT technique compared to dispersion curves from the best models. The observed value is shown as a black line. The bottom panel shows the shear velocity averaged over the upper 30 (x), 40 (+), 60 (triangle), and 80 km (circle) of all GA searched models.

3 which uses Criteria 3 in its GA search gets 4 votes for scheme 1 , and 1 point for scheme 2; the other 3 tests get 0 votes under either scheme. We now restart the GA search process for 17 initial models for each of the four
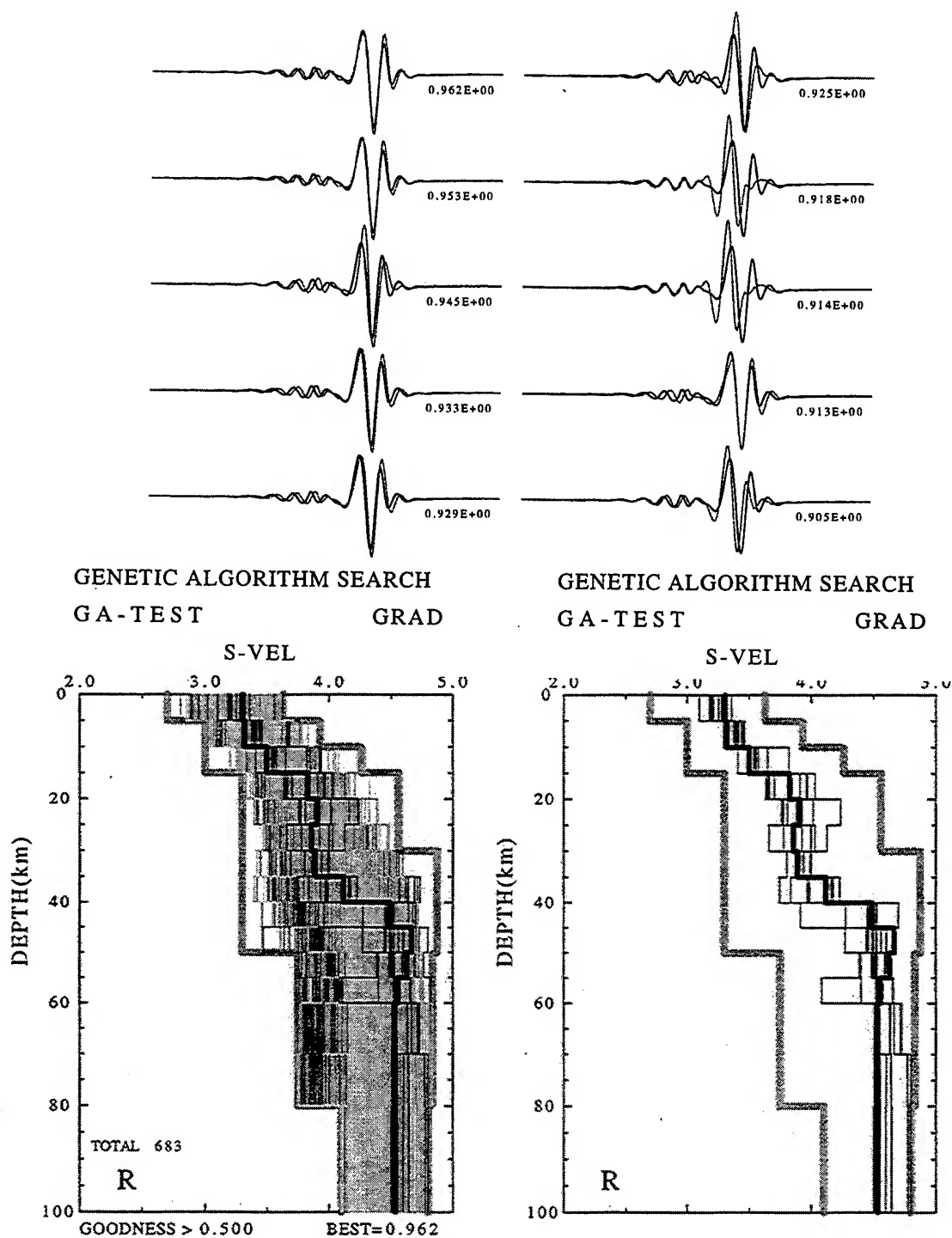
Figure 10. GA search results using Criteria 2. See Figure 7 for explanation.

goodness of fit criteria. The composite tally of votes is given in Table 2.
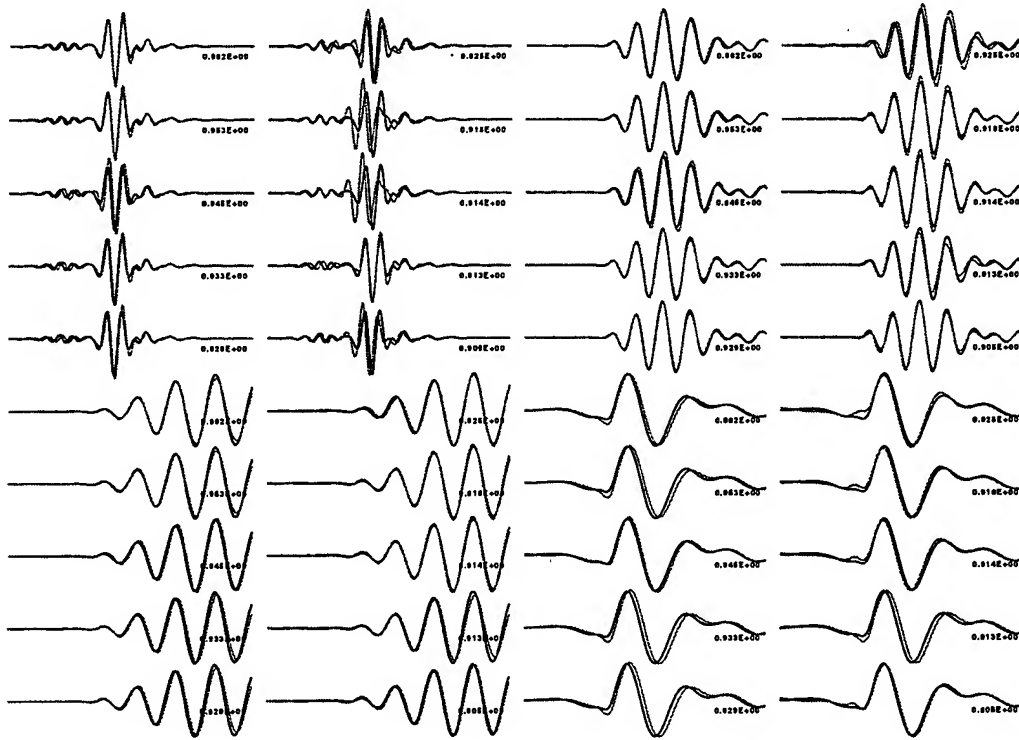
Figure 11. Seismogram comparison for ten best GA searched models using Criteria 2. See Figure 8 for explanation.

Table 2. The result of 17 experiments evaluated by 2 schemes

	criteria 1	criteria 2	criteria 3	criteria 4
scheme 1	12	20	22	15
scheme 2	4	8	6	4

In Table 2, we can see that Criteria 2 and 3 are roughly equivalent and are better than Criteria 1 and 4 in determining a good model.

Why does Criteria 2 seems to be better than Criteria 1? It must be due to reasons that force the hyper-surface of the object function to be smoother than the others. Therefore, the GA evolution mechanism will gradually approach the best goodness region without much trouble. Although it is impossible to show the object function surface because it is a multi-dimensional surface, it is also impossible to evaluate such a surface for the infinite number of models that need to be computed. All we can say is that the object function is smoother in some over-simplified cases that we can compute. For example, if observed and synthetic seismograms are very similar to each
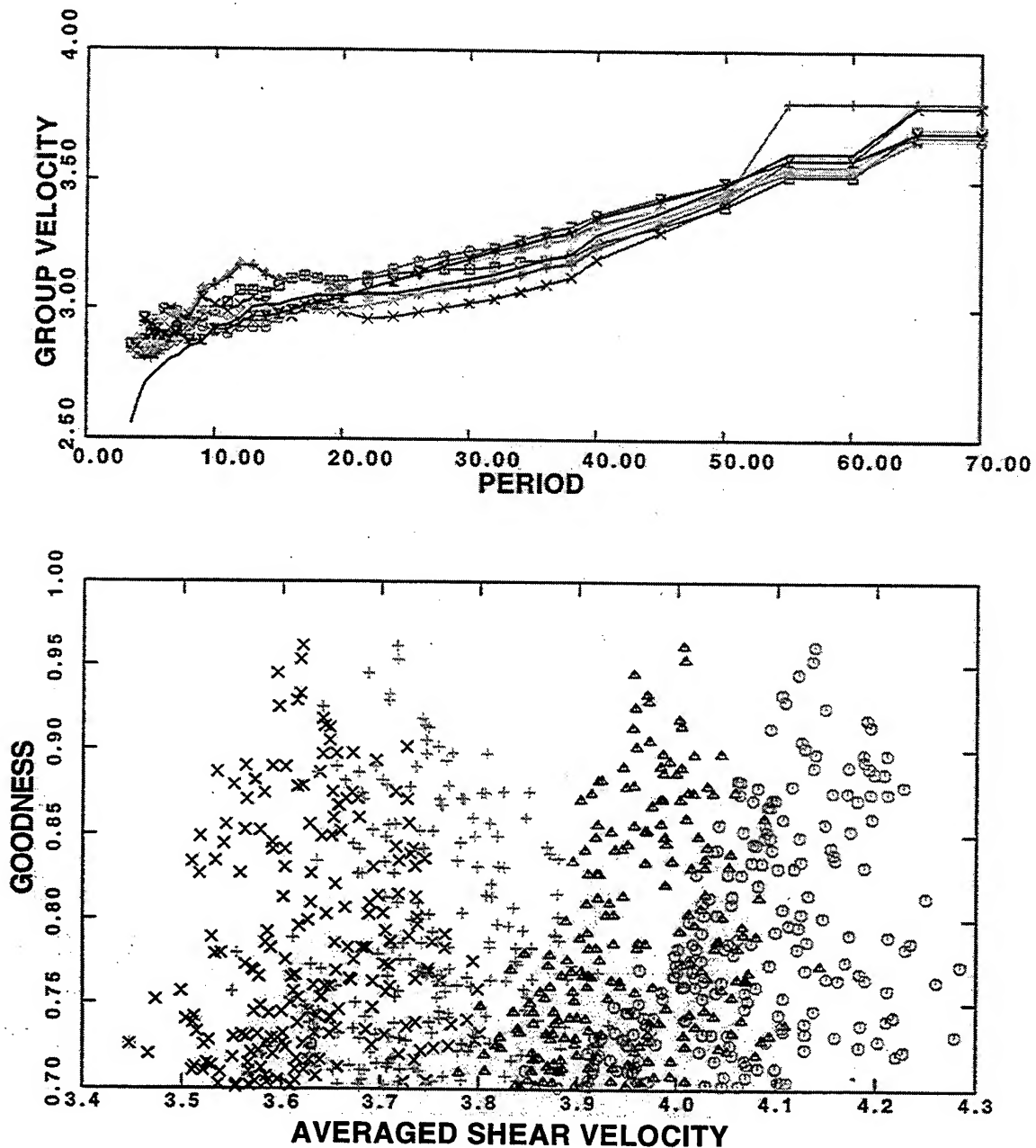
Figure 12. Uncertainty for the second GA search test. See Figure 9 for explanation.

other with only some time-shift between them, we can see the object function of Criteria 2 is smoother than the object function of Criteria 1.

To illustrate this, we use a synthetic seismogram in Figure 19 for our "observed" data and shift this seismogram for our "synthetic" data and evaluate the goodness values for four different criteria. The bottom panel shows
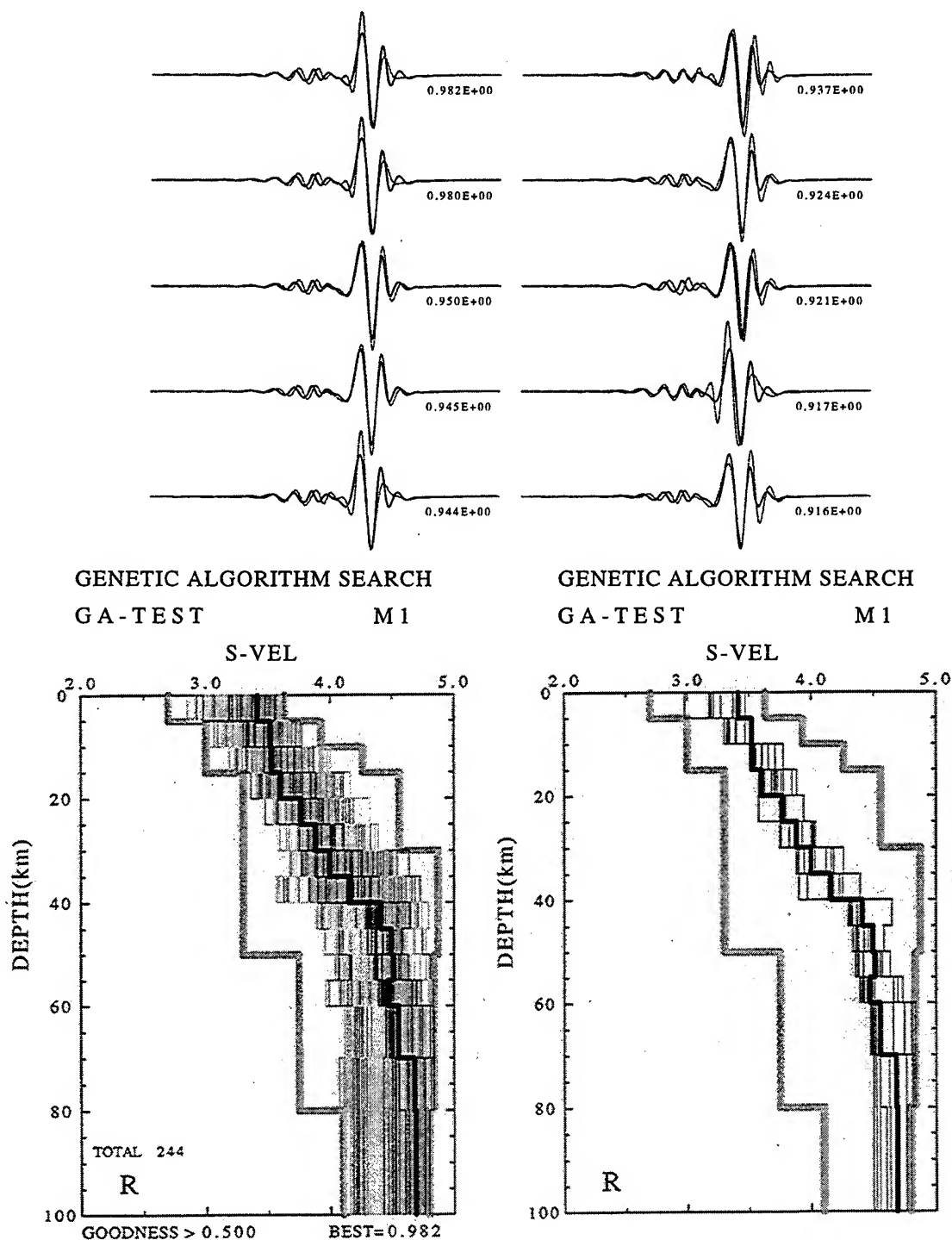
Figure 13. GA search results using Criteria 3. See Figure 7 for explanation.

these four object functions: as a funtion of time shift for Criteria 1, Criteria 2, Criteria 3 and Criteria 4. We can see that three of them have a very sharp

Figure 14. Seismogram comparison for ten best GA searched models which using Criteria 3. See Figure 8 for explanation.

narrow range of high goodness values. This is mostly controlled by the periodic behavior of the L1, L2 based norms and the cross-correlation values. However, Criteria 2, which only uses the group and phase velocity information, has a broader and smoother range of goodness values which means it is more tolerant of time shifts than the other three criteria.

2.7 Conclusion

In this study, we designed four criteria for modeling surface-wave waveforms. These four criteria were designed using some directly measurable quantities such as L1 and L2 norms, normalized cross-correlation value at zero time lag, and time shift information of maximum envelope and maximum amplitude of cross-correlation. These four criteria were tested using the genetic algorithm search method for 17 repeated experiments. Each experiment consisted of four GA runs with different criteria.

The results suggest that the second criteria, which only uses group and phase velocity information, is the best for modeling surface-wave waveforms. The other three criteria may be influenced by the periodic behavior of the L1 and L2 norms and cross-correlation value and have smaller and narrower regions of high goodness values. This means the second criteria is more
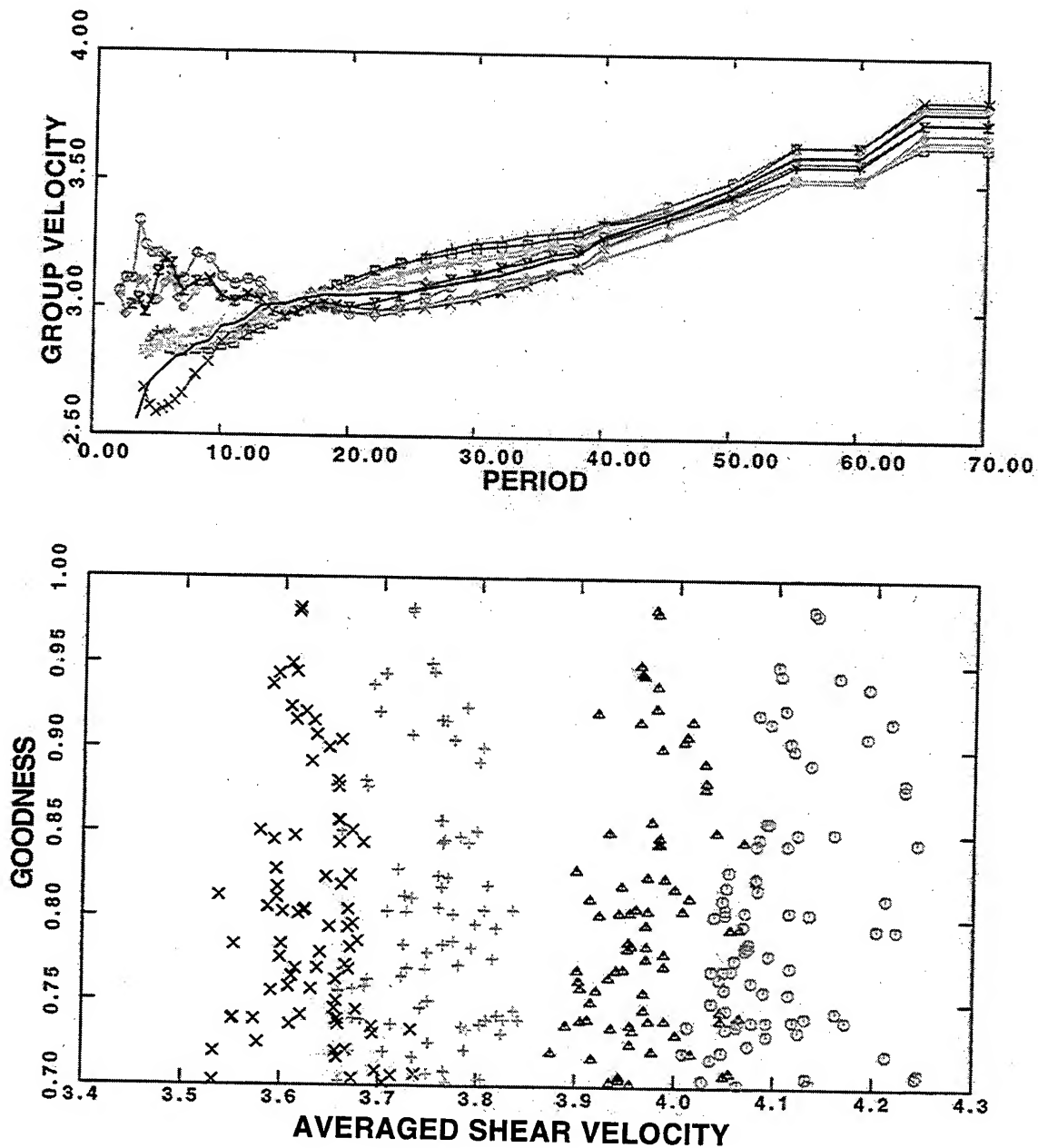
Figure 15. Uncertainty for the third GA search test. See Figure 9 for explanation.

tolerant of incorrect models and can still use information of those models in the evolution process of genetic algorithm.

Although we only performed 17 experiments, and this may not be enough from a statistical viewpoint, we believe the result of this study is an initial step in searching for a good criteria for use in modeling complicated seismic

waveforms.

GENETIC ALGORITHM SEARCH

GA-TEST   M 1

GENETIC ALGORITHM SEARCH

GA-TEST   M 1
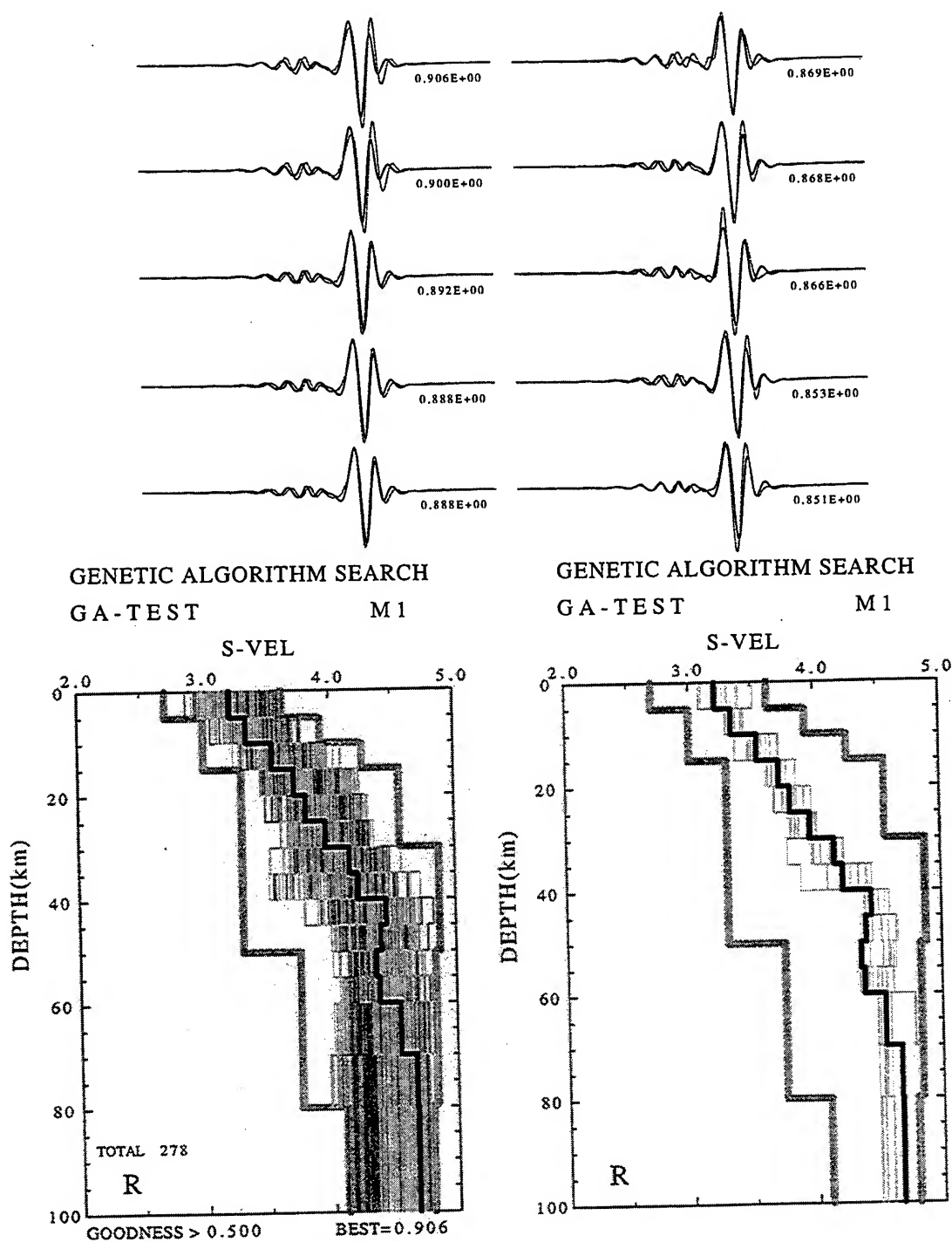
Figure 16. GA search results for using criteria 4. See Figure 7 for explanation.
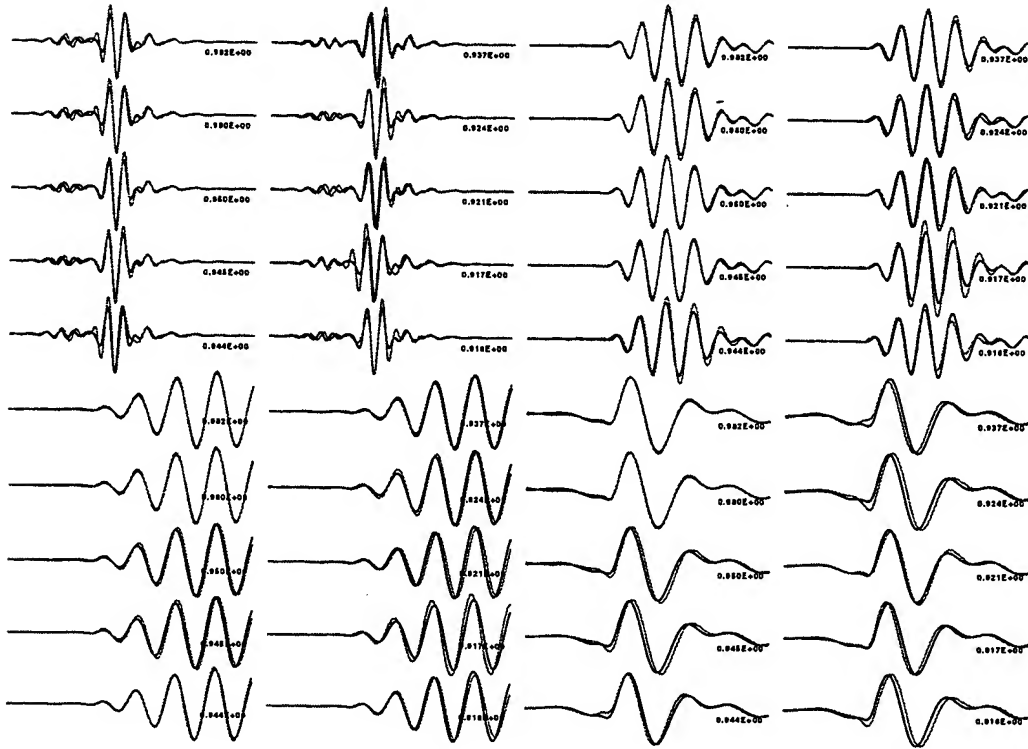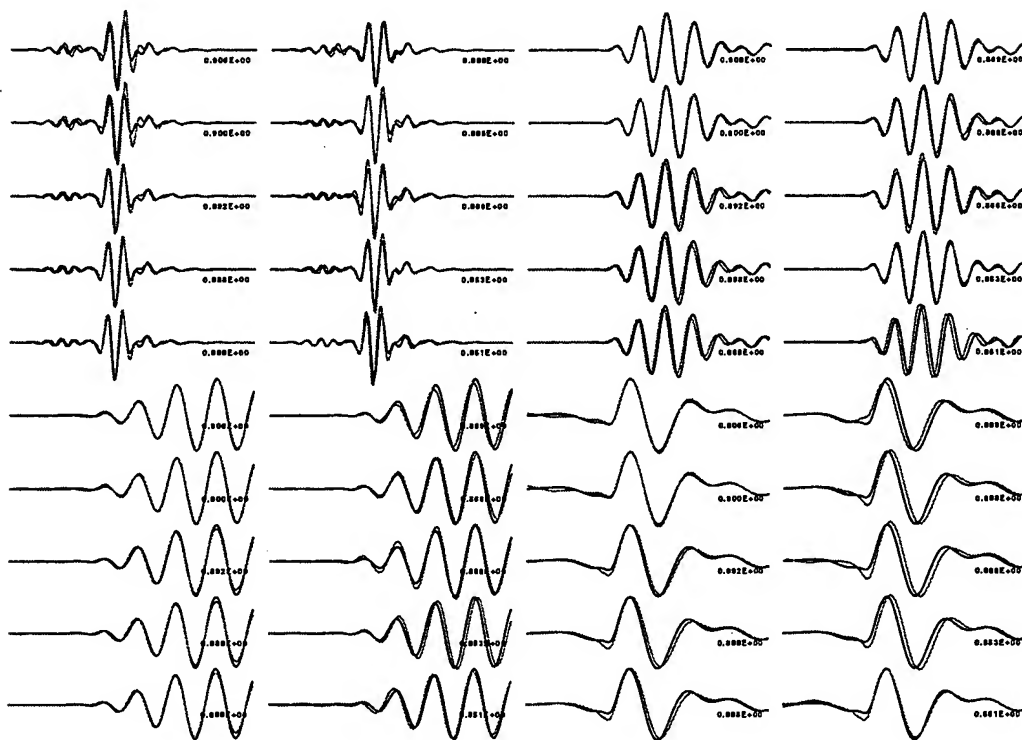
Figure 17. Seismogram comparison for ten best GA searched models using criteria 4. See Figure 8 for explanation.
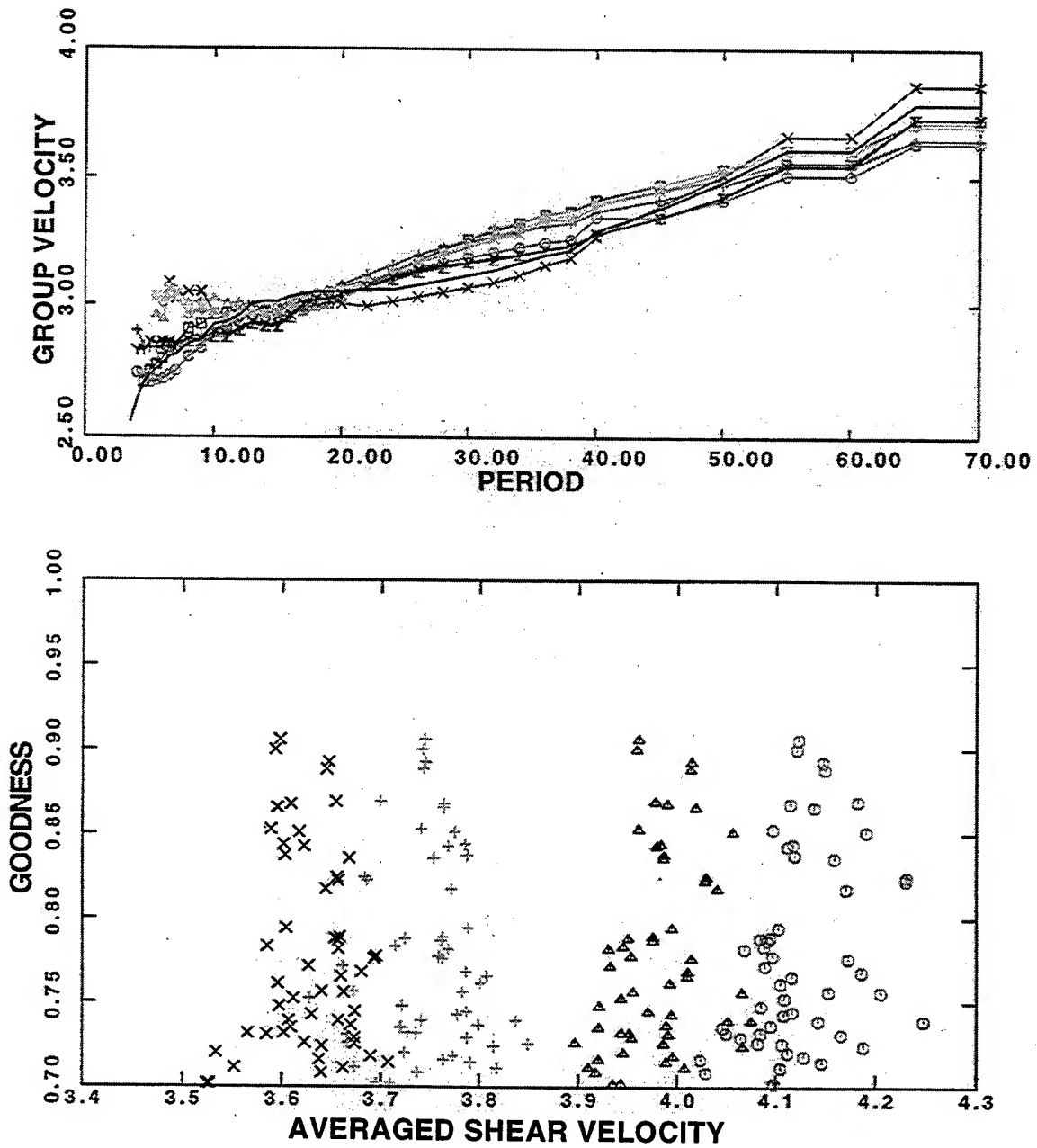
Figure 18. Uncertainty for fourth GA search test. See Figure 9 for explanation.
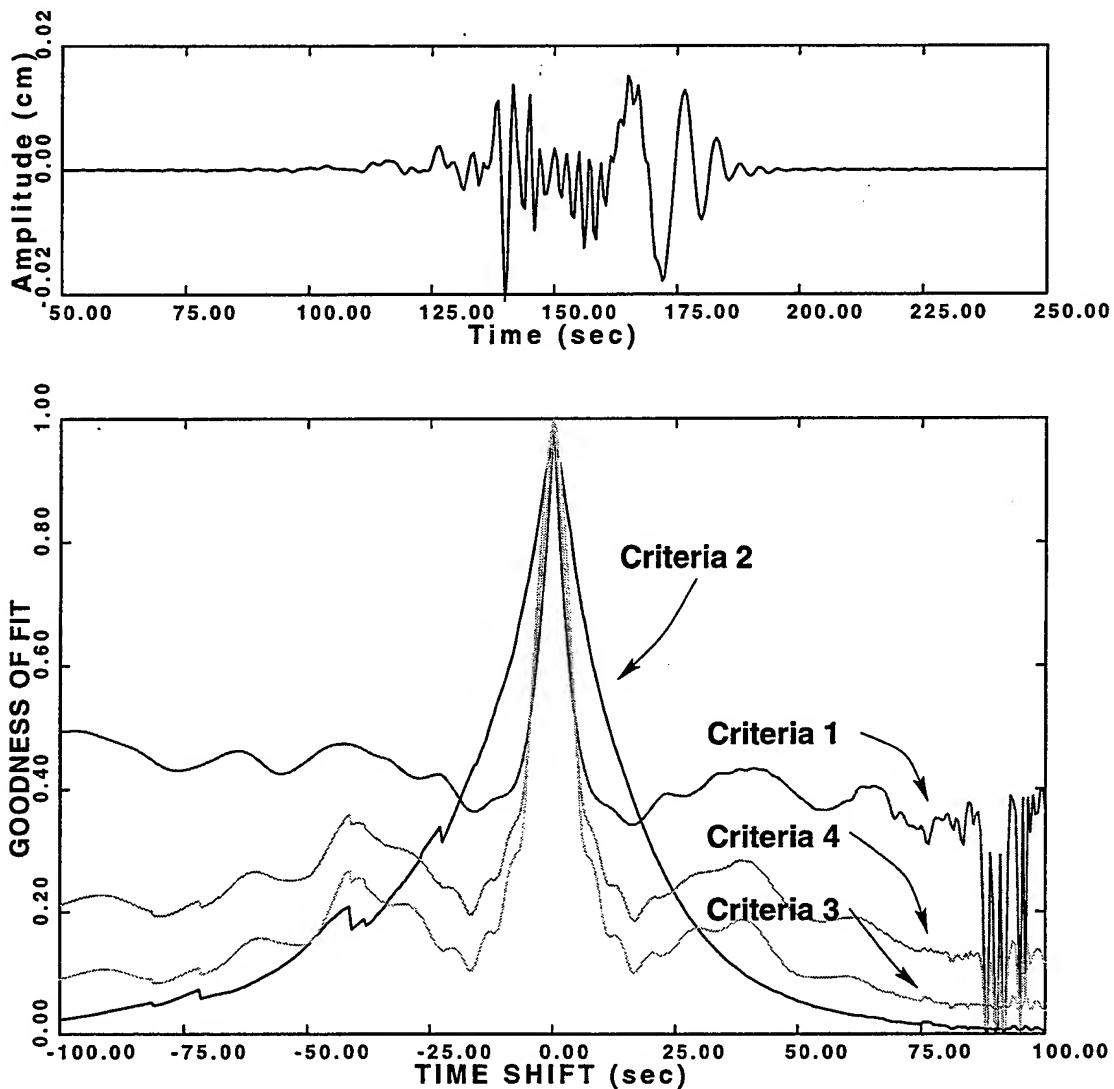
Figure 19. Illustration of object functions for four different criteria in an over-simplified case. See text for detail.

2.8 References

Cara, M., and J. J. Leveque (1987). Waveform inversion using secondary observables, *Geophys. Res. Lett.,* **14,** 1046-1049.

Dziewonski, A. M., S. Bloch, and M. Landisman (1969). A technique for the analysis of transient seismic signals, *Bull. Seis. Soc. Am.,* **59,** 427-444.

Herrmann, R. B.(1973). Some aspects of band-pass filtering of surface waves, *Bull. Seis. Soc. Am.,* **63,** 663-671.

Lerner-Lam, A. L. and T. H. Jordan (1983). Earth structure from

fundamental and higher-mode waveform analysis, *Geophys. J. R. astr. Soc.*, **75,** 759-797.

Zhao, L-S., and D. V. Helmberger (1994). Source estimation from broadband regional seismograms, *Bull. Seis. Soc. Am.*, **84,** 91-104.

Zhu, L., and D. V. Helmberger (1996). Advancement in source estimation techniques using broadband regional seismograms, *Bull. Seis. Soc. Am.*, **86,** 1634-1641.

3. MODELING SURFACE-WAVE WAVEFORMS USING A GENETIC ALGORITHM

Tao-Ming Chang and Robert B. Herrmann

3.1 Abstract

We apply a genetic algorithm search method to model regional surface-wave waveforms. In this application, we use some seismological constraints to regulate the test models which improve the use for small population sizes (20 individuals) and short numbers of generations (50 generations). The waveform goodness-of-fit is based on measurements of travel time differences of normalized cross-correlation of observed and synthetic seismograms that have been narrow-band filtered in subranges of the period interval of interest. The synthetic tests show our application of the genetic algorithm search method can successfully find several good final models that can be used as input for further detailed studies. The real data tests have been applied to data from the 1995 West Texas earthquake and have shown a satisfactory waveform fit. We have not found a good way to quantify the uncertainty of the genetic algorithm search method, but provide an indirect way to represent the uncertainty qualitatively.

3.2 Introduction

Most seismological inverse problems are nonlinear. The techniques used to solve such nonlinear problems can be placed into two groups. The strategy of the first is to linearize nonlinear problems, then use iterative processes to seek a better solution by using the gradient information of the hypersurface of the misfit function. The strategy of the second is to directly search the model space and find the acceptable models.

Methods such as least squares, steepest descents, and conjugate gradient belong to the first group. Although these methods are widely used in seismology, the requirement of a good starting model is a well-known disadvantage. For studying large scale, long wavelength features or deep features beneath the lithosphere, this would not be a real problem because the research of the past half century already provides some good starting models, e.g., PREM (Dziewonski and Anderson, 1981) and IASPEI91 (Kennett and Engdahl, 1991). On the other hand, for studying crustal or lithospheric structure, a good starting model may not be available because the crust or lithosphere is the most structurally heterogeneous region in the Earth. We must investigate the structure of the crust and lithosphere all over the world to study its evolutionary history, to understand the tectonic processes, to better predict seismic activity, and to lower the damage of earthquake hazards.

Therefore, it is necessary to find a way to investigate many possible models, that is, to search the whole model space and to select the acceptable models of structure and their variations. The Monte Carlo, simulated annealing (SA), and genetic algorithms (GA) search methods belong to this group. The

Monte Carlo method is a random search method that has been used in seismology for a long time (for example, by Keilis-Borok and Yanovskaja, 1967; Press, 1968). Press (1968) showed a successful experiment that used the Monte Carlo method to search for the model that can produce correct body-wave travel-times, surface-wave dispersion, the earth's free oscillation periods, mass, and moment of inertia. Six models were found from about five million randomly generated models. Examining these six models, we find that the structures for the lower mantle are consistent, but that large fluctuations occur in the upper mantle (lithosphere). As pointed out by Press (1968), the reason for using the Monte Carlo method is that it offers the advantage of exploring the range of possible solutions and indicates the degree of uniqueness achievable with currently available geophysical data. However, the Monte Carlo method has its own disadvantages. As discussed by Keilis-Borok and Yanovskaja (1967), the Monte Carlo method does not use information obtained from previous trials in the next trial.

Recently, two better search algorithms which utilize the information of previous trials, simulated annealing and genetic algorithms, have become very popular in seismology. The simulated annealing method mimics the crystallizing process observed in chemistry. The genetic algorithm is inspired by the evolution process observed in biological science. The seismological applications have been the estimation of residual statics (Rothman, 1985, 1986; Wilson and Vasudevan, 1991), waveform inversion of reflection data (Sen and Stoffa, 1991, 1992; Stoffa and Sen, 1991; Sambridge and Drijkoningen, 1992; Drijkoningen and White, 1995), earthquake hypocenter location determination (Sambridge and Gallagher, 1993), receiver function inversion (Shibutani, Sambridge, and Kennett, 1996; Zhao et al., 1996; Nerves et al., 1996), determination of earthquake source parameters (Hartzell and Liu, 1995; Zeng and Anderson, 1996; Kobayashi and Nakanishi, 1994), estimation of the source time function (Courboulex et al., 1996). Simulated annealing and genetic algorithms have also been used to study many different type of data such as teleseismic P waves (Steck, 1995; Zhou et al., 1995), surface-wave dispersion data (Lomax and Snieder, 1994, 1995; Yamanaka and Ishida, 1996), and seismic exploration data (Jervis et al., 1993, 1996; Jin and Madariaga, 1994; Mallick, 1995; Nolte and Frazer, 1994), and other applications (Pullammanappallil and Louie, 1994; Riepl et al., 1995; Vasudevan et al.; Velis and Ulrych, 1996). There is one thing in common in all these applications: they all deal with nonlinear problems (Scales et al., 1992; Gallagher et al., 1991). In addition to their wide range of applications in seismology, GA and SA may also provide an intuitive way to analyze the error or uncertainty. For example, in receiver function inversion, Ammon et al. (1990) showed that the final models were dependent on the initial models. Shibutani et al. (1996) showed that genetic algorithm can estimate an average model which is more stable and less dependent on the starting model.

We see the goal of the global search techniques is to obtain several good starting models and the uncertainty range, which will then be refined using using iterative waveform inversion techniques. In this paper, we will focus on several topics to explain why we study the surface wave, why we use the genetic algorithm instead of simulated annealing, and what our purposes and expectations are.

3.3 Purpose

At present the Genetic Algorithm has been applied in many topics in seismology such as hypocenter location determination, receiver function inversion, estimation of the source time function and surface wave dispersion data inversion. But, the results show there is no guarantee of reaching global minimum by using GA. So, the proper questions about the use of GA in seismology are: What is the strength of genetic algorithm method? What can be accomplished by using GA? How do we utilize this tool?

In this study, we use GA as a tool to quickly delineate the possible models for surface-wave waveform modeling. Under some reasonable *a priori* conditions, we use GA to search the model space and to determine a few good starting models for other waveform inversion algorithms which are better for such a task.

Because the genetic algorithm crudely searches the model space, the search results can be used to show the possible ranges of uncertainty. This is important because most goodness-of-fit measures used in seismology are not useful in indicating the actual uncertainties. For example, in damped least square inversion, the resolving kernel and standard deviation are dependent on the damping value. It is possible to adjust the damping value and show a different range of uncertainty. Therefore, it would be better to have the search results indicate the possible uncertainty. In this study, we plot the search results to show the deviation range of models. Although we can only provide qualitative instead of quantitative information, such presentation will provide intuitive information in the manner of the "checker board" test used in tomographic inversion. Also, as pointed out by Sambridge and Drijkoningen (1992), the development of error analysis for a GA search remains a great challenge if one is only to rely on GA.

3.4 Why Study Surface Waves?

As stated previously, the main goal is to establish a set of algorithms for studying lithospheric structure. Although different seismic phases can be used for such a task, we select surface waves for several major reasons. First of all, high quality surface-wave data are easily obtainable because of widely deployed broadband instruments. For most shallow earthquakes, the surface wave usually has a higher signal/noise ratio than the body-wave signal. Second, for any local small aperture broadband seismic network, the records may form a huge database for studying the regional structure. However, the

difficulty in such research is that signals may have a higher frequency content than signals used in global tomography studies. At these higher frequencies, the surface wave travels mostly through the crust which is the most heterogeneous part of the earth. It is really necessary to have a method to obtain reasonable starting models for detailed waveform modeling. Finally, since surface waves sample the near surface structure, modeling surface waves using a 1-D model can provide an average structure. Although this does not sound exciting, it should serve as the foundation for studying complicated 3-D structures. As an analogy, seismic exploration, researchers are trying to extract background velocity (1-D), and use it as a starting point for studying more complicated structures (Koren et al., 1991; Bunks et al., 1995; Lauda et al., 1989).

Here, we also would like to explain why are we using surface-wave waveform data instead of dispersion data. Theoretically, if the data have a high S/N ratio, the waveform and dispersion data should be equally suitable for inversion. There are some reasons for us to use the waveform data. First, there has been a tremendous improvement in computation ability. Calculating synthetic seismograms may only take seconds instead of the hours previously. Second, the dispersion data were usually obtained using the multiple filter analysis technique. Sometimes unavoidable measuring errors will be introduced in such measuring procedures. In order to get the phase velocity data, another measuring process such as a phase matched filter is necessary. Of course, some artifacts may be introduced. It is very difficult to identify the dispersion for higher modes. We will try to find a good way to extract information directly from the waveform to avoid these problems.

3.5 Comparison of SA and GA

From the variety of applications in earthquake and exploration seismology, we find that both simulated annealing (SA) and genetic algorithms (GA) are good ways to perform the uncertainty assessment in a complicated nonlinear problem. The algorithm chosen depends on the characteristics of problem. As stated by Sambridge and Drijkoningen (1992) concerning the SA and GA methods: "any problem feasible by one could also be tackled by the other". To distinguish which of the two methods (GA or SA) is better for the surface-wave waveform modeling problem, we need to understand both algorithms and the purpose of our application. As is well known, generating multi-mode surface-wave synthetics is computationally intensive. Therefore, the computation time will be a crucial factor for selection of the algorithm. Of course, there are some applications of an artificial neural network algorithm in seismology (Leach et al., 1993; McCormack et al., 1993; Paulli and Dysart, 1990; Wang and Teng, 1995, 1997; Wang and Mendel, 1992) but they are less popular than GA and SA and may require very large training sets.

3.5.1 Workflow of Simulated Annealing Method

The computational procedure of simulated annealing consists of the following steps:

- start from an arbitrary model

- temperature-loop : at temperature $T = T_0 - k \cdot \delta T$
  - □ parameter-loop : for model parameter $S_i, i = 1, \cdots, m$

    fix all other parameter value except S_i

    for the parameter S_i, there are n possible values.
      - ○ possible-value-loop : $S_{ij}, j = 1, \cdots, n$

        calculate an energy function $E(S_{ij})$ (the normalized cross-correlation of observed and synthetic seismogram is one example)
      - ○ end of possible-value-loop
  - □ end of parameter-loop

    compute the probability distribution

$$P(S_{ij}) = \frac{\exp[\dfrac{-E(S_{ij})}{T}]}{\sum\limits_{j=1}^{m} \exp[\dfrac{-E(S_{ij})}{T}]} \tag{13}$$

- end of temperature-loop

We can see that for each temperature, it is necessary to perform $(m \cdot n)$ forward computations of synthetics. If there are k steps in lowering temperature to reach the global minimum, the total forward computation will be $(k \cdot m \cdot n)$. The problem is that there is no rule for choosing the starting temperature T_0 and increment of temperature difference δT. Basu and Frazer (1990) designed a sequence of test runs to find the critical temperature. In spite of this, it is still too time-consuming for surface-wave waveform modeling.

3.5.2 Workflow of the Genetic Algorithm

For an m member society evolving through n generation, the computational sequence of the genetic algorithm is as follows:

- Randomly generate m individual models as the first generation.

- Generation-loop : for *generation* $= 1, \cdots, n$

  Compute m synthetic seismograms (individuals)

  Evaluate each individual's performance; i.e. calculate the goodness-of-fit.
  - □ population-loop : for *child* $= 1, \cdots, m$

    Based on the individuals' performance (probability)

    select them as parents;

    change parents' DNA; and

apply possible mutation on their children.

    □ end of population-loop

•   end of generation-loop

We see it is possible to perform GA on a small population. This will be computationally more efficient than SA in the surface-wave waveform modeling problem. However, performing GA on a small population society has its own risk, as pointed out by Sambridge and Drijkoningen (1992). If the society's members are not close to the global solution, the few relatively good individuals in the society will multiply themselves and dominate the population (that is, the solution will be trapped in a local minimum leading to premature selection). This problem can be addressed by increasing the population size. However, our purpose for using GA in surface-wave waveform modeling is not to rely on the GA to reach the global minimum. Instead, we prefer to have several runs to see the possible uncertainty, get a rough idea about the structure, and find some good initial models for other inversion techniques. In our test, a GA run will take 1 to 3 hours of CPU time on a 167 MHz workstation. It is affordable to have several reruns if we find it trapped in a local minimum.

We thus select the genetic algorithm for modeling surface-wave waveforms.

3.6 Technical

The basic concepts of the genetic algorithm are well presented by other authors (e.g. Sambridge and Drijkoningen, 1992; Stoffa and Sen, 1991). Here we will only address the technical issues in implementing GA to surface-wave waveform modeling.

3.6.1 Generation Number and Population Size

Although GA is a global search method which can potentially find the global minimum, we did not set that as the goal in this study. Due to the intensive computational load of generating multi-mode surface-wave synthetics, we limited our computations to a small population size and propagated it through only a finite number of generations. We hoped, by using the GA search method, to get some starting models for other inversion algorithms. To understand what generation number is sufficient for our purpose, we have tested the consequences of a large generation number. In this test, with results shown in Figure 20a, we propagated 500 generations and find that after 50 generations model improvement is less rapid, indicating a degree of convergence. Therefore, in the subsequent tests, we will only use 50 generations for a small population (20). This will only consume 1 to 3 hours of CPU time on a 167 MHz workstation. In Figure 20b, we perform four repeated
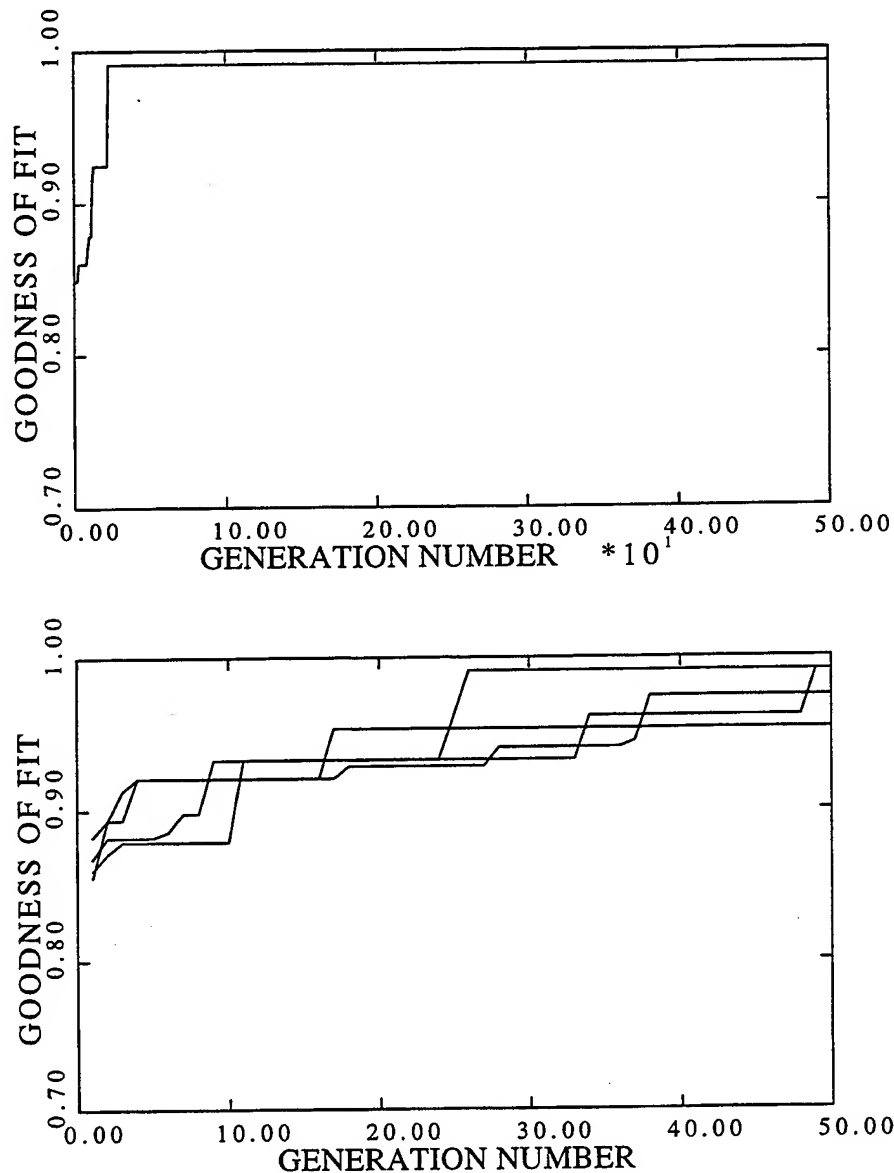
Figure 20. (a) Top panel. This experiment shows the best fitness found by a small popula-
tion (20 individuals) GA search through 500 generations. The result shows that 50 genera-
tions is acceptable for the reason of saving computation time. (b) bottom panel. Comparison
of 4 separate GA searches. Again, the 50 generation limit seems acceptable.

experiments and show their best fitness values through 50 generations. The
experiments show that the GA search method is reliable and repeated experi-
ments show similar evolution trends.

3.6.2 Smoothing Mechanism or Model Generating Mechanism

The GA searches the model space randomly, therefore it has an advantage that a broad range of models can be tested and it is possible to reach the global minimum if the problem has been properly formulated and the search process has lasted long enough. However, because of its random search behavior, many unreasonable models can be generated which are not acceptable under seismological constraints. In this study, we found it necessary to use some seismological constraints to regulate the randomly generated models. We call this process "smoothing". This process will help the GA find many "reasonable" models in such a short run for the small population size described previously. This smoothing concept is not new to this report; rather, several papers already mention similar ideas. For example, Lomax and Snieder (1995) used a "centrally weighted five-point" smoothing mechanism to smooth over their 18-node velocity profiles. Another example is from Sambridge and Drijkoningen (1992), who allow only models which have positive velocity gradients to be generated when they modeled marine seismic refraction waveforms. Although these smoothing mechanisms depend on the parametrization, we believe this concept will be very important for seismologists who wish to apply GA to other seismological problems. Therefore we will briefly describe the smoothing process. First, we need to define a "reasonable model". For a regional shallow event, the surface wave can probably only resolve the crustal structure. When low-pass-filtered the surface wave signal is a simple pulse. We will not see very detailed structure by modeling such signals. Under such limitations, we can only hope to find some velocity models that vary simply with depth. For this study, this is our definition of "reasonable model".

As shown in Figure 21, the free parameters will randomly generate models with inherent "zig-zag" behavior. Because of the period range of surface wave and the scale of structure, we wish to use a smooth velocity-depth curve instead of randomly generated models with a "zig-zag" pattern. Therefore, we smooth it in two ways that will be chosen randomly. The first way is to reduce the velocity contrast between any two adjacent layers without changing the total vertical travel time. The second way is to use a center-weighted triangular shape moving over the velocity profile to smooth the velocity model. This is similar to the smoothing mechanism used by Lomax and Snieder (1995).

A constraint was used to check the validity of such a model. From most published models, we conclude that it is valid that the average velocity of the upper crust is lower than the average velocity of lower crust, that the average upper mantle velocity is faster than the average lower crust velocity, and that the upper mantle does not have strong velocity gradients. For example, if the Moho depth is 40 km, we will divide the first 100 km into four layers: layer 1
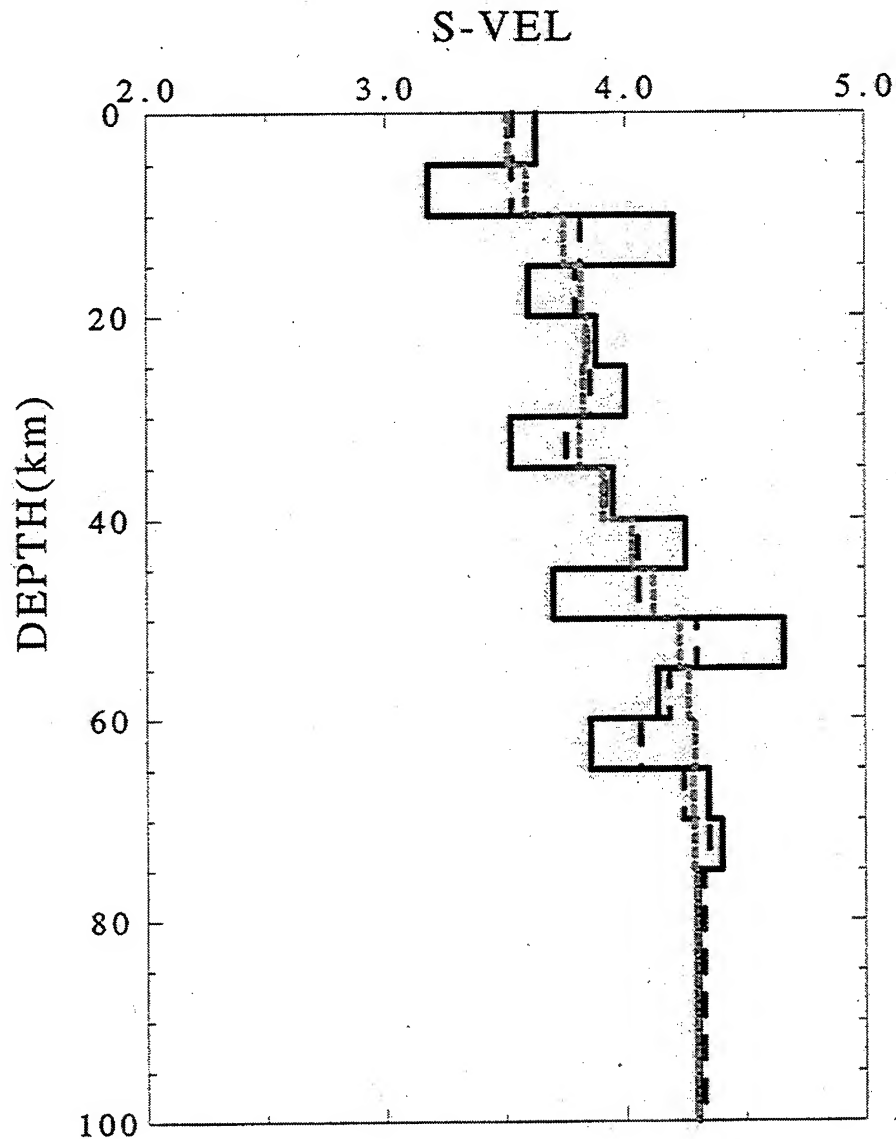
Figure 21. This figure shows how the smoothing mechanisms smooth the randomly generated model (solid line) which always has a strong "zig-zag" pattern. The long dashed line shows the smoothed result by reducing velocity contrast. The short dashed line shows the smoothed result by moving a center-weighted triangular weighting function over the model.

(0-20 km; upper crust), layer 2 (20-40 km; lower crust), layer 3 (40-60 km; upper mantle), layer 4 (60-100 km). The average velocity for the first three layers should increase monotonically, and the average velocity of the fourth layer should not deviate too much from the third layer (typically, it should be within 0.15 km/sec).

As mentioned previously, the surface-wave period range generated by a regional shallow event may provide very little resolution for structure deeper

43

than the Moho. However, it is necessary to provide the deeper structure to fit higher modes or for modeling teleseismic seismograms. For this part of the velocity model, we do not generate it randomly. Instead, we construct a sequence of models (Figure 22) based on the SNA, TNA (Grand and Helmberger, 1984), and IASP91 models (Kennett and Engdahl, 1991). The deeper model selected will be based on the average velocity of the fourth layer (usually 60-100 km) mentioned previously.

3.6.3 The Criteria of Goodness-of-Fit

In GA, the goodness-of-fit criteria is user defined. It is a subjective criteria of goodness-of-fit for modeling surface waves. To start the design of the criteria, it is necessary to understand the characteristics of the object that will be modeled.

There are two major characteristics of a surface wave. First, a surface-wave signal has a longer duration and a more complicated waveform behavior than any single, pulse-like body-wave phase. When modeling such long-duration complicated waveforms, there is a cycle-skipping problem which may produce an unreasonably low or high velocity model. In addition, when processing surface-wave data, we cannot shift synthetic seismograms to match the observed arrival time, a well adapted technique in receiver function inversion of body wave data. Therefore, the cycle-skipping problem will be the first problem to be resolved. Second, surface-waves usually have a broad frequency content. Any single measurement from a waveform may not be adequate to represent the whole waveform because of the frequency dependence of the signal content. For example, a single cross-correlation measurement only represents the similarity of the shape of the largest amplitudes, which are typically high-frequency for shallow crustal earthquakes. This will only resolve the very shallow part of the structure but leave the deeper structure uncertain with high variation.

To overcome these two problems, we design our criteria of waveform goodness-of-fit as

$$\left\{ \left[\prod_{j=1}^{n} \left(\frac{1}{1 + \left| \frac{3.5 * (TS_c)_j}{dist} \right|} \right)^{10} \right]^{1/n} \cdot \left[\prod_{j=1}^{n} \left(\frac{1}{1 + \left| \frac{3.5 * (TS_u)_j}{dist} \right|} \right)^{10} \right]^{1/n} \right\}^{1/2} \qquad (14)$$

First we divided period range of interest into several subranges and narrow bandpass-filter observed and synthetic seismograms for each subrange. For example, for a regional seismogram, we divided the period range (10-50 sec) into 4 intervals : (10-20 sec), (20-30 sec), (30-40 sec), and (40-50 sec). For each subrange period interval, we compute the cross-correlation of these narrowband filtered observed and synthetic seismograms. After that, two important
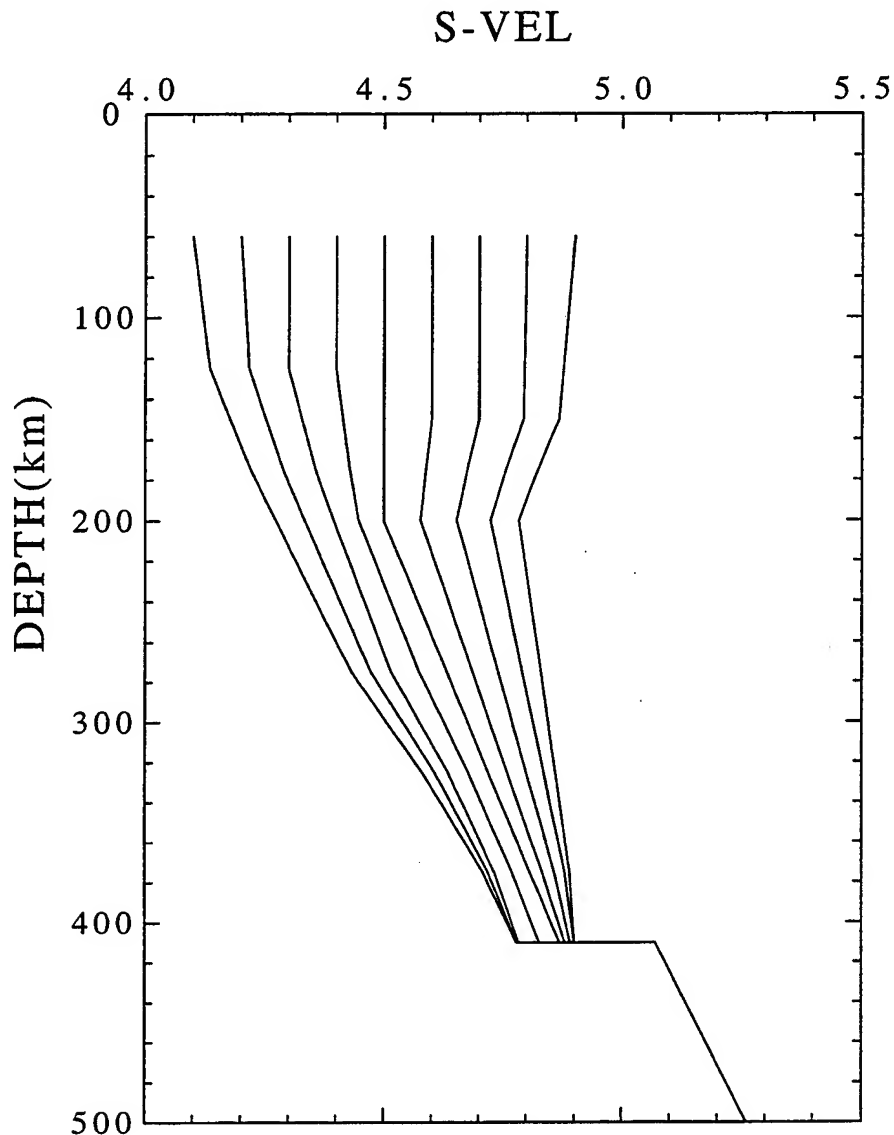
Figure 22. Because the surface-wave generated by shallow focus earthquakes usually do not generate much long-period signal that can be used to resolve the deep structure, it is necessary to ensure that the deep part of the model be able to model teleseismic seismograms. We construct a sequence of possible models which are based on SNA, TNA, and IASPEI91 models for the GA search method.

time shift parameters can be measured: the time shift of the envelope of cross-correlation (TS_u) and the time shift of maximum cross-correlation (TS_c). These two measurements are similar to surface-wave group and phase velocity differences between observed and synthetic seismograms. Assuming that the averaged surface-wave traveling speed is 3.5 km/sec and using epicentral distance (*dist*), we can roughly estimate the percentage of travel time

difference between observed and synthetic seismograms. Finally, the value of goodness-of-fit can be calculated. When TS_c and TS_u approach zero for each subrange, we can assume that a good solution has been found and its goodness-of-fit is close to one. Otherwise, the exponential term in (13) will pull the goodness-of-fit away from unity for just a few percent travel time difference. This criteria will also tolerate an incorrect Q model used to generate a synthetic seismogram because it is based on the normalized cross-correlation measurements.

3.7 Synthetic Test

We conducted several synthetic tests to examine the suitability of the GA search method. Firstly, correct and incorrect crustal Q models have been tested. In our experiment, we set averaged crustal $Q_s = 800$, which deviated 100% from the correct $Q_s = 400$. As discussed in the previous section, the criteria of goodness-of-fit is based on normalized cross-correlation measurements, therefore it won't show too much difference for the two cases. Secondly, we have tested the consequence of using Butterworth and Gaussian filters. The results show roughly the same results for both filters. From these two experiments, we conclude that the design of goodness-of-fit criteria is very robust. The success of the GA search method depends only on the mechanism of the genetic algorithm (that is, selection, exchange DNA, and mutation) or the mechanism of generating models (that is, smoothing, parameterization).

We also conducted a test to see whether the GA search method has the ability to distinguish between a gradient Moho and a sharp Moho. Figures 23 and 24 show the GA searched results for synthetic gradient Moho and sharp Moho. These tests assume the receiver is 500 km away from the source and that we have imperfect knowledge about crustal Q models. Each figure has three small plots. The top panel shows the ten best search results (gray line) compared with "observed" seismogram (black line) with their fitness value on the right; the displayed time interval is from 50 to 250 seconds. The bottom right plot shows these ten searched models (light gray line), the best model (solid black line), the "true" model (black dashed line), and search bound (thick dark gray line). Although, these ten models have somewhat good waveform fits when judged visually, their models span a certain width on each layer which may be used as an indicator for uncertainty. For example, the uncertainty around the Moho is large in comparison to other depths. This indicates that the surface wave has very little ability to resolve Moho structure for such a short distance (500 km) and period range (10-100 sec). Also, the top layer of very low velocity sediment is not resolvable from this period range. The bottom left plots of Figures 23 and 24 show those search models that have their goodness-of-fit value greater than a certain threshold. The color indicating different goodness-of-fit values, for example very dark gray

for those model greater equal 0.9, medium gray for those between 0.7 and 0.9, gray for those between 0.5 and 0.7, and light gray for those below 0.5. From these experiments, we conclude that the GA search method can roughly resolve the shear velocity structure, but it needs more *a priori* knowledge to resolve the top sediment layer and Moho structure.
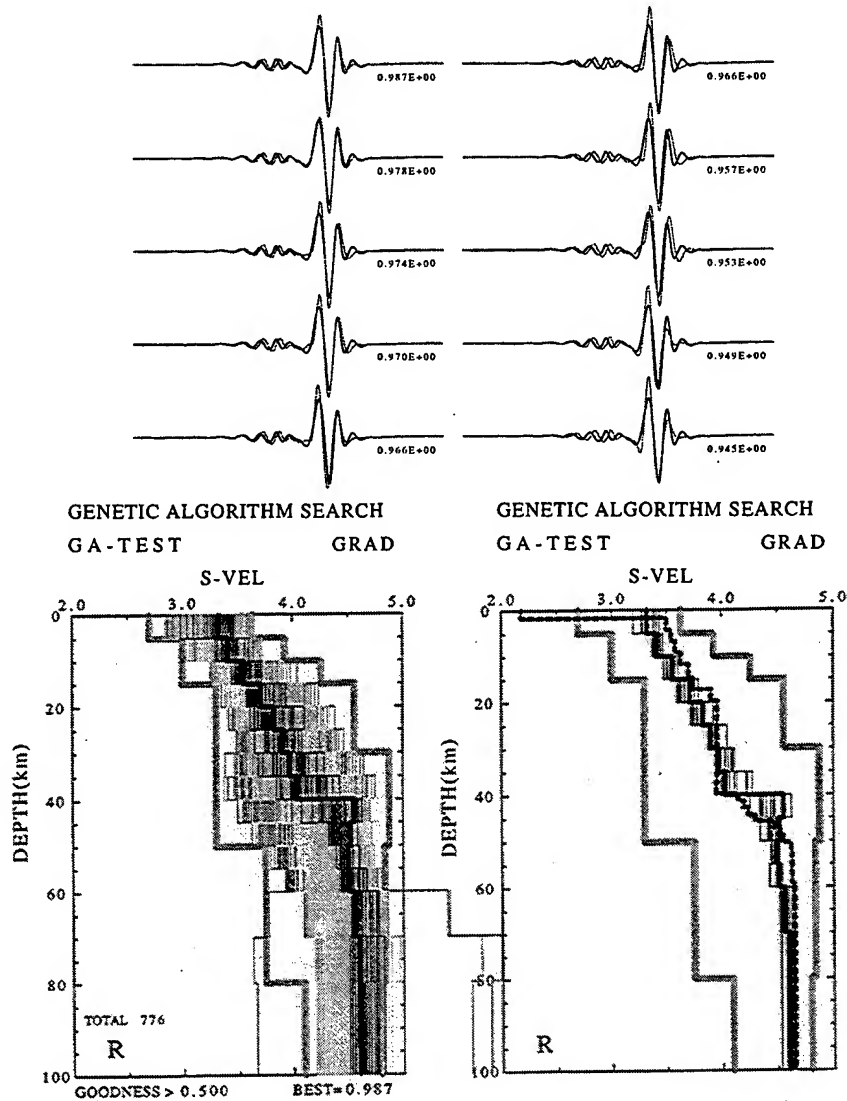
Figure 23. This figure shows GA test results for a gradient Moho model. The top panel shows waveform comparison (gray) for ten best searched models with their goodness-of-fit values on the right, against the original waveform (black). The bottom right plot shows the search bounds (outer gray), the "true" model (black dashed), ten best models (light gray), and the best model (black). The bottom left plot shows most models with lighter color, indicating a better goodness-of-fit value. See text for details.

Figure 24. This figure shows GA test results for a sharp Moho model. See Figure 23 for explanations and text for details.

3.8 Real Data Test (1995 Texas Earthquake)

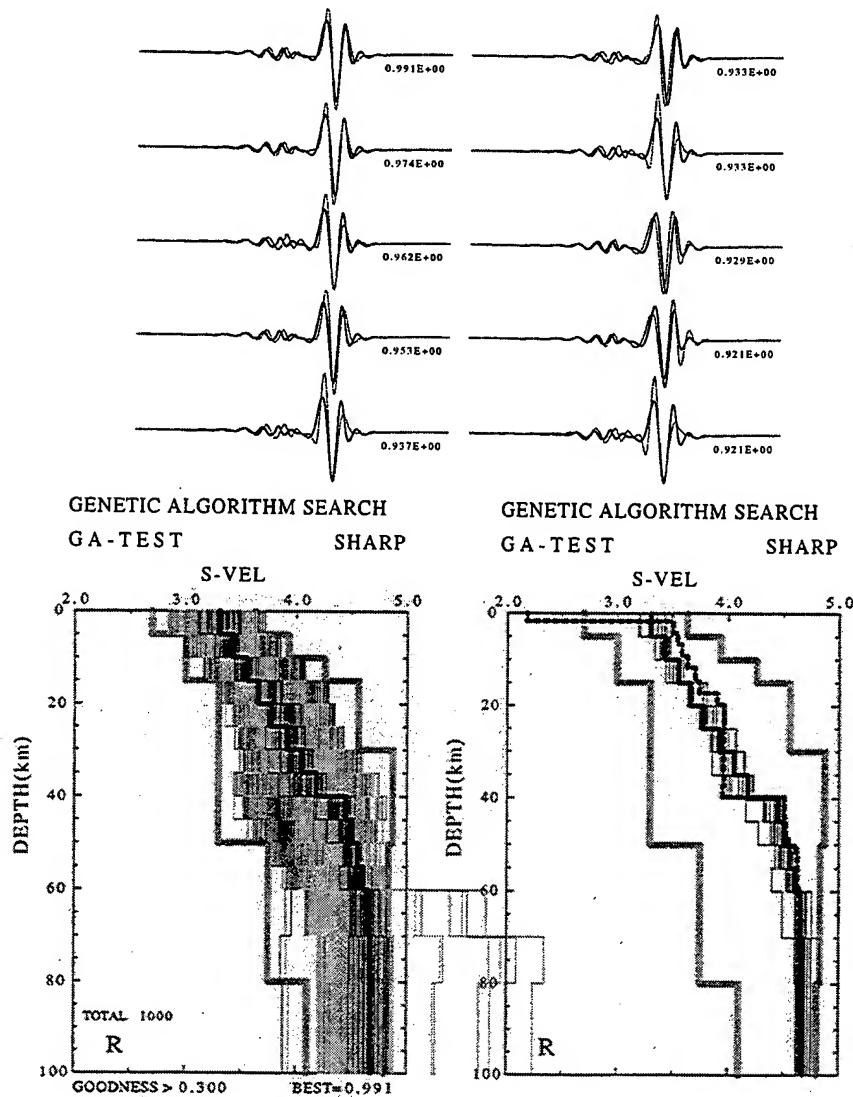We wish now to apply the GA search method to real data. We selected the April 14, 1995 western Texas earthquake to test. Here we will show the search results for two stations (WMOK and FCC) which have very different epicentral distances, 655 and 3244 km, respectively. Figure 25 shows the GA search results for WMOK. The displayed seismograms are filtered between 10-100 seconds and cut between 100-300 seconds after origin time. From the bottom right plot, we see that the search results have a large uncertainty for structure below 40 km and a slightly lower velocity for the deeper part. This is reasonable because the observed data do not have enough long-period

signal to resolve the deep structures. However, if we focus on the shallow part of the models, we see well-resolved shear velocity structure for the top 30 km which is contributed by the strong fundamental mode. The flaw of this search result is that none of the best ten models can fit the higher modes well. The GA model solution may be used as a starting point for other inversion techniques.

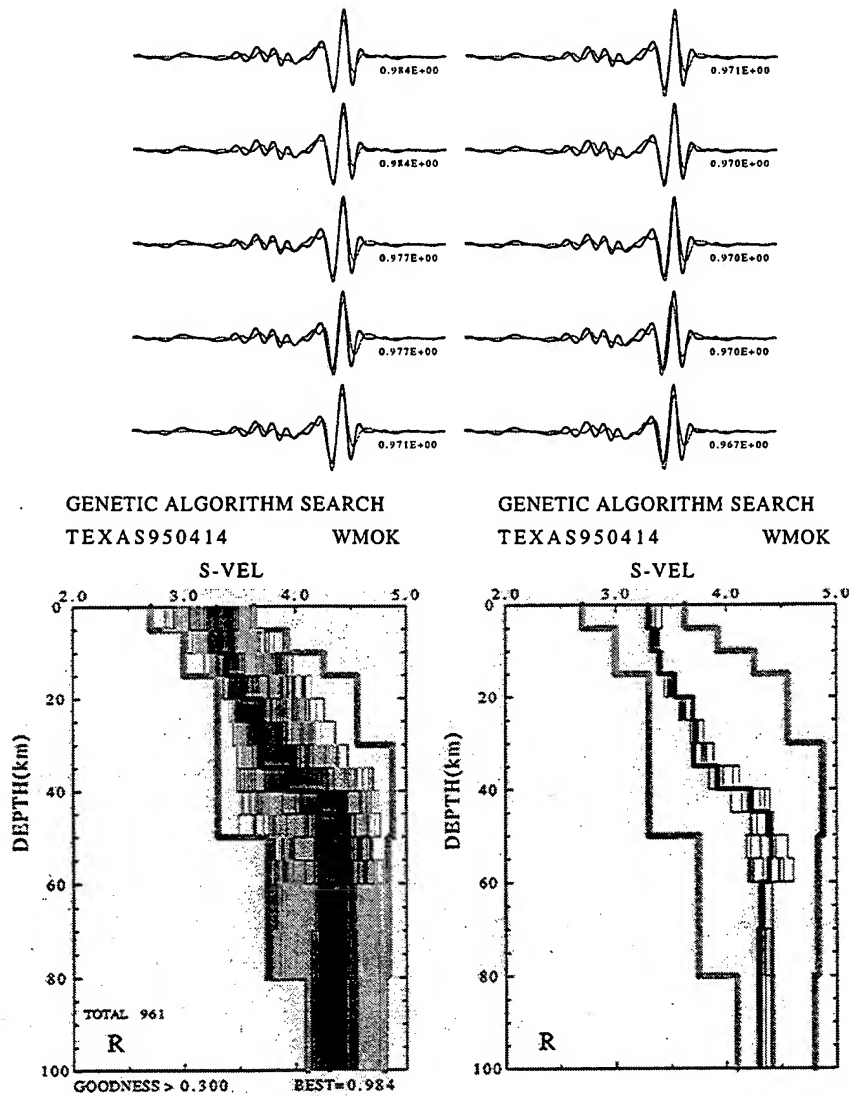Figure 25. This figure shows GA search results for WMOK. See Figure 23 for explanations and text for details.

Figure 26 shows the GA search results for FCC. The displayed seismograms are filtered between 20-100 seconds and cut to 750-1300 seconds after origin time. In this search, we divided the period interval of interest (10-100 sec) into four sub-intervals: (10-20 sec), (20-35 sec), (35-60 sec), and (60-100

sec). The search results do not fit the observed waveform perfectly. The best model has the correct velocity for the low frequency signals which means the deep structure of its model is close to the truth but it fails to produce the correct amplitude around the Airy phase. The tenth model has the correct amplitude and envelope shape around the Airy phase but fails to fit the long-period part. Therefore, we see all ten best search results could be used as a starting point for more detailed studies of waveform behavior.
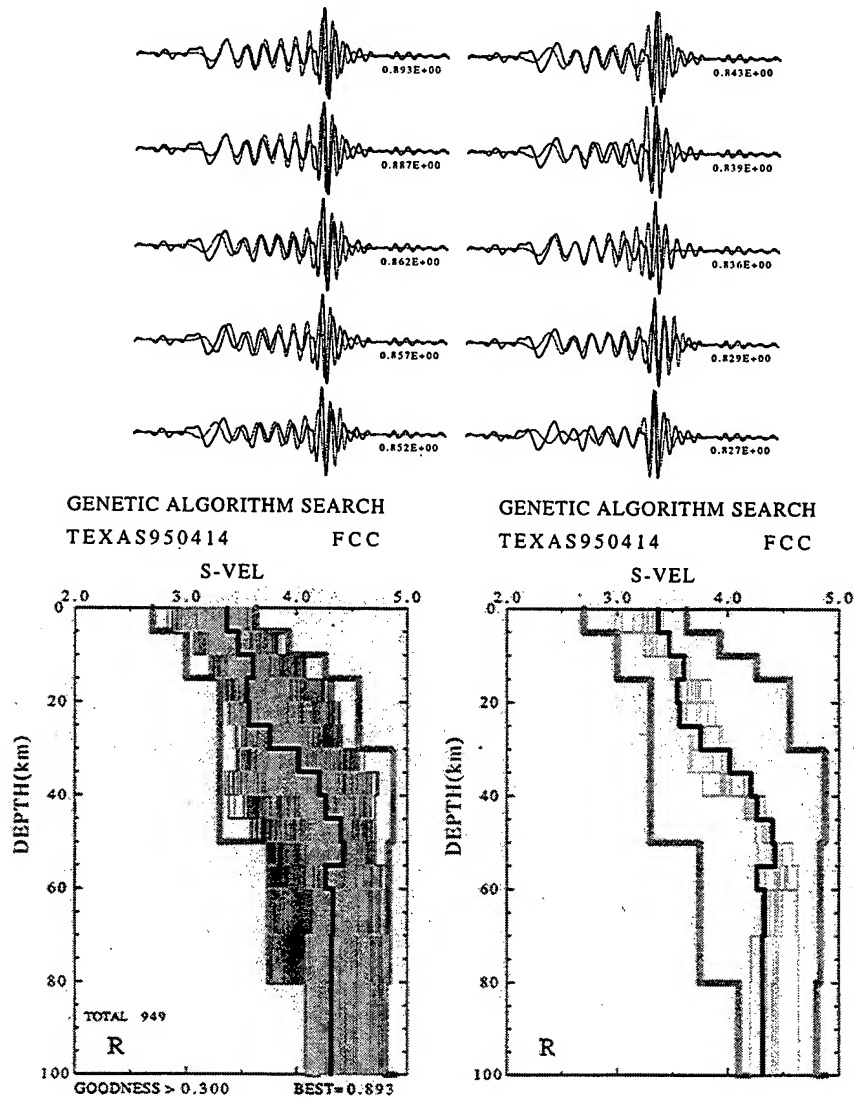

Figure 26. This figure show GA searched results for FCC. See Figure 23 for explanations and text for details.

3.9 Discussion

This study has shown that the GA search method is capable of finding several models that can fit the surface-wave waveform reasonably well. The GA search method can be applied to regional and teleseismic records because we construct a sequence of models for the deep structures. This method is very fast and therefore is practical for application to real earthquake data. The search models can be used as starting models for other detailed studies. The research goal has been fulfilled successfully. Although there is no quantitative method for defining the uncertainty of searched results, several suggestions have been made for indirect measures.

What is the weakness of this tool? It is obvious that not all of the searches will be successful. Although we believe our criteria of goodness-of-fit is very tolerant of an incorrect Q model and is reasonably well behaved, it definitely is not the perfect one. That is why the GA search will sometimes yield excellent results and sometimes not. In this study, we feel that the finding of final good solutions is more dependent on the model-generating mechanism than on the mechanism of the genetic algorithm (evolution process). In other words, the more seismological constraints that have been applied, the greater efficiency and accuracy of the process. Also, if we know more about waveform behavior, we may design a more intelligent and efficient guided search method.

3.10 References

Ammon, C. J., G. E. Randall, and G. Zandt, 1990. On the nonuniqueness of receiver function inversions, *J. Geophys. Res.*, **95**, 15303-15318.

Basu, A., and L. N. Frazer, 1990. Rapid determination of the critical temperature in simulated annealing inversion, *Science*, **249**, 1409-1412.

Bunks, C., F. M. Saleck, S. Zaleski, and G. Chavent, 1995. Multiscale seismic waveform inversion, *Geophysics*, **60**, 1457-1473.

Courboulex, F., J. Virieux, and D. Gilbert, 1996. On the use of simulated annealing method and cross-validation theory for deconvolution of seismograms, *Bull. Seis. Soc. Am.*, **86**, 1187-1193.

Drijkoningen, G. G., and R. S. White, 1995. Seismic velocity structure of oceanic crust by inversion using genetic algorithms, *Geophys. J. Int.*, **123**, 653-664.

Dziewonski, A. M., and D. L. Anderson, 1981. Preliminary reference earth model, *Phys. Earth Planet. Int.*, **25**, 297-356.

Gallagher, K., M. Sambridge, and G. Drijkoningen, 1991. Genetic algorithm: an evolution from Monte Carlo methods for strongly non-linear geophysical optimization problems, *Geophys. Res. Lett.*, **18**, 2177-2180.

Grand, S. P., and D. V. Helmberger, 1984. Upper mantle shear structure of North America, *Geophys. J. R. astr. Soc.*, **76**, 399-438.

Hartzell, S., and P. Liu, 1995. Determination of earthquake source parameters using a hybrid global search algorithm, *Bull. Seis. Soc. Am.*, **85,** 516-524.

Jervis, M., M. K. Sen, and P. L. Stoffa, 1996. Prestack migration velocity estimation using nonlinear methods, *Geophysics*, **61,** 138-150.

Jervis, M., P. L. Stoffa, and M. K. Sen, 1993. 2-D migration velocity estimation using a genetic algorithm, *Geophys. Res. Lett.,* **20,** 1495-1498.

Jin, S., and R. Madariaga, 1994. Nonlinear velocity inversion by a two-step Monte Carlo method, *Geophysics,* **59,** 577-590.

Keilis-Borok, V. I., and T. B. Yanovskaja, 1967. Inverse problem of seismology (structural review), *Geophys. J. R. astr. Soc.,* **13,** 223-234.

Kennett, B. L. N., and E. R. Engdahl, 1991. Traveltimes for global earthquake location and phase identification, *Geophys. J. Int.,* **105,** 429-465.

Kobayashi, R., and I. Nakanishi, 1994. Application of genetic algorithm to focal mechanism determination, *Geophys. Res. Lett.,* **21,** 729-732.

Koren, Z., K. Mosegaard, E. Landa, P. Thore, and A. Tarantola, 1991. Monte Carlo estimation and resolution analysis of seismic background velocities, *J. Geophys. Res.,* **96,** 20289-20299.

Lauda, E, W. Beydoun, and A. Tarantola, 1989. Reference velocity model estimation from prestack waveform: coherency optimization by simulated annealing, *Geophysics,* **54,** 984-990.

Leach, R. R., F. U. Dowla, and E. S. Vergino, 1993. Yield estimation using bandpass-filtered seismograms: preliminary results using Neural Networks with *mb(Pn),* short-time, long-time, and coda energy measurements, *Bull. Seis. Soc. Am.,* **83,** 488-508.

Lomax, A. J., and R. Snieder, 1994. Finding sets of acceptable solutions with a generic algorithm with application to surface wave group dispersion in Europe, *Geophys. Res. Lett.,* **21,** 2617-2620.

Lomax, A., and R. Snieder, 1995. The contrast in upper mantle shear-wave velocity between the east European platform and tectonic Europe obtained with genetic algorithm inversion of Rayleigh-wave group dispersion, *Geophys. J. Int,* **123,** 169-182.

Mallick, S., 1995. Model-based inversion of amplitude-variations-with-offset data using a genetic algorithm, *Geophysics,* **60,** 939-954.

McCormack, M. D., D. E. Zaucha, and D. W. Dushek, 1993. First-break refraction event picking and seismic data trace editing using neural networks, *Geophysics,* **58,** 67-78.

Nerves, F. A., S. C. Singh, and K. F. Priestley, 1996. Velocity structure of upper-mantle transition zones beneath central Eurasia from seismic inversion using genetic algorithms, *Geophys. J. Int.,* **125,** 869-878.

Nolte, B., and L. N. Frazer, 1994. Vertical seismic profile inversion with genetic algorithms, *Geophys. J. Int.,* **117,** 162-178.

Paulli, J. J., and P. S. Dysart, 1990. An experiment in the use of trained

neural networks for regional seismic event classification, *Geophys. Res. Lett.,* **17,** 977-980.

Pullammanappallil, S. K., and J. N. Louie, 1994. A generalized simulated-annealing optimization for inversion of first-arrival times, *Bull. Seis. Soc. Am.,* **84,** 1397-1409.

Riepl, J., A. Rietbrock, and F. Scherbaum, 1995. Site response modeling by non-linear waveform inversion, *Geophys. Res. Lett.,* **22,** 199-202.

Rothman, D. H., 1986. Automatic estimation of large residual statics corrections, *Geophysics,* **51,** 332-346.

Rothman, D. H., 1985. Nonlinear inversion, statistical mechanics, and residual statics estimation, *Geophysics,* **50,** 2784-2796.

Press, F., 1968. Earth models obtained by Monte Carlo inversion, *J. Geophys. Res.,* **73,** 5223-5234.

Sambridge, M., and K. Gallagher, 1993. Earthquake hypocenter location using genetic algorithms, *Bull. Seis. Soc. Am.,* **83,** 1467-1491.

Scales, J. A., M. L. Smith, and T. L. Fischer, 1992. Global optimization methods for multimodal inverse problems, *J. Comp. Phys.,* **103,** 258-268.

Sen, M. K., and P. L. Stoffa, 1991. Nonlinear one-dimensional seismic waveform inversion using simulated annealing, *Geophysics,* **56,** 1624-1638.

Sen, M. K., and P. L. Stoffa, 1992. Rapid sampling of model space using genetic algorithms: examples from seismic waveform inversion, *Geophys. J. Int.,* **108,** 281-292.

Steck, L. K., 1995. Simulated annealing inversion of teleseismic P-wave slowness and azimuth for crustal structure at Long Valley Caldera, *Geophys. Res. Lett.,* **22,** 497-500.

Stoffa, P. L., and M. K. Sen, 1991. Nonlinear multiparameter optimization using genetic algorithms: inversion of plane-wave seismograms, *Geophysics,* **56,** 1794-1810.

Vasudevan, K., W. G. Wilson, and W. G. Laidlaw, 1991. Simulated annealing statics computation using an order-based energy function, *Geophysics,* **56,** 1831-1839.

Velis, D. R., and T. J. Ulrych, 1996. Simulated annealing wavelet estimation via fourth-order cumulant matching, *Geophysics,* **61,** 1939-1948.

Wang, J., and T-L. Teng, 1995. Artificial neural network-based seismic detector, *Bull. Seis. Soc. Am.,* **85.,** 308-319.

Wang, J., and T-L. Teng, 1997. Identification and picking of S phase using an artificial neural network, *Bull. Seis. Soc. Am.,* **87,** 1140-1149.

Wang, L. X., and J. M. Mendel, 1992. Adaptive minimum prediction-error deconvolution and source wavelet estimation using Hopfield neural network, *Geophysics,* **57,** 670-679.

Wilson, W. G., and K. Vasudevan, 1991. Application of the genetic algorithm to residual statics estimation, *Geophys. Res. Lett.,* **18,** 2181-2184.

Yamanaka, H., and H. Ishida, 1996. Application of genetic algorithms to an

inversion of surface-wave dispersion data, *Bull. Seis. Soc. Am.,* **86,** 436-444.

Zeng, Y., and J. G. Anderson, 1996. A composite source model of the 1994 Northridge earthquake using genetic algorithms, *Bull. Seis. Soc. Am.,* **86,** S71-S83.

Zhao, L. S., M. K. Sen, P. Stoffa, and C. Frohlich, 1996. Application of very fast simulated annealing to the determination of the crustal structure beneath Tibet, *Geophys. J. Int.,* **125,** 355-370.

Zhou, R., F. Tajima, and P. L. Stoffa, 1995. Application of genetic algorithms to constrain near-source velocity structure for the 1989 Sichuan Earthquakes, *Bull. Seis. Soc. Am.,* **85,** 590-605.

THOMAS AHRENS
SEISMOLOGICAL LABORATORY 252-21
CALIFORNIA INST. OF TECHNOLOGY
PASADENA, CA 91125

AIR FORCE RESEARCH LABORATORY
ATTN: VSOP
29 RANDOLPH ROAD
HANSCOM AFB, MA 01731-3010   (2 COPIES)

AIR FORCE RESEARCH LABORATORY
ATTN: RESEARCH LIBRARY/TL
5 WRIGHT STREET
HANSCOM AFB, MA 01731-3004

AIR FORCE RESEARCH LABORATORY
ATTN: AFRL/SUL
3550 ABERDEEN AVE SE
KIRTLAND AFB, NM 87117-5776 (2 COPIES)

RALPH ALEWINE
NTPO
1901 N. MOORE STREET, SUITE 609
ARLINGTON, VA 22209

G. ELI BAKER
MAXWELL TECHNOLOGIES
8888 BALBOA AVE.
SAN DIEGO, CA 92123-1506

MUAWIA BARAZANGI
INSTOC
3126 SNEE HALL
CORNELL UNIVERSITY
ITHACA, NY 14853

DOUGLAS BAUMGARDT
ENSCO INC.
5400 PORT ROYAL ROAD
SPRINGFIELD, VA 22151

THERON J. BENNETT
MAXWELL TECHNOLOGIES
11800 SUNRISE VALLEY
SUITE 1212
RESTON, VA 22091

WILLIAM BENSON
NAS/COS
ROOM HA372
2001 WISCONSIN AVE. NW
WASHINGTON DC 20007

JONATHAN BERGER
UNIV. OF CALIFORNIA, SAN DIEGO
SCRIPPS INST. OF OCEANOGRAPHY IGPP, 0225
9500 GILMAN DRIVE
LA JOLLA, CA 92093-0225

ROBERT BLANDFORD
AFTAC
1300 N. 17TH STREET
SUITE 1450
ARLINGTON, VA 22209-2308

LESLIE A. CASEY
DEPT. OF ENERGY/NN-20
1000 INDEPENDENCE AVE. SW
WASHINGTON DC 20585-0420

CENTER FOR MONITORING RESEARCH
ATTN: LIBRARIAN
1300 N. 17th STREET, SUITE 1450
ARLINGTON, VA 22209

FRANCESCA CHAVEZ
LOS ALAMOS NATIONAL LAB
P.O. BOX 1663, MS-D460
LOS ALAMOS, NM 87545   (5 COPIES)

ANTON DAINTY
DTRA/PMA
45045 AVIATION DRIVE
DULLESVA 20166-7517

CATHERINE DE GROOT-HEDLIN
UNIV. OF CALIFORNIA, SAN DIEGO
IGPP
8604 LA JOLLA SHORES DRIVE
SAN DIEGO, CA 92093

DIANE DOSER
DEPT. OF GEOLOGICAL SCIENCES
THE UNIVERSITY OF TEXAS AT EL PASO
EL PASO, TX 79968

DTIC
8725 JOHN J. KINGMAN ROAD
FT BELVOIR, VA 22060-6218 (2 COPIES)

MARK D. FISK
MISSION RESEARCH CORPORATION
735 STATE STREET
P.O. DRAWER 719
SANTA BARBARA, CA 93102-0719

LORI GRANT
MULTIMAX, INC.
311C FOREST AVE. SUITE 3
PACIFIC GROVE, CA 93950

HENRY GRAY
SMU STATISTICS DEPARTMENT
P.O. BOX 750302
DALLAS, TX 75275-0302

I. N. GUPTA
MULTIMAX, INC.
1441 MCCORMICK DRIVE
LARGO, MD 20774

DAVID HARKRIDER
BOSTON COLLEGE
24 MARTHA'S PT. RD.
CONCORD, MA 01742

THOMAS HEARN
NEW MEXICO STATE UNIVERSITY
DEPARTMENT OF PHYSICS
LAS CRUCES, NM 88003

MICHAEL HEDLIN
UNIVERSITY OF CALIFORNIA, SAN DIEGO
SCRIPPS INST. OF OCEANOGRAPHY
9500 GILMAN DRIVE
LA JOLLA, CA 92093-0225

DONALD HELMBERGER
CALIFORNIA INST. OF TECHNOLOGY
DIV. OF GEOL. & PLANETARY SCIENCES
SEISMOLOGICAL LABORATORY
PASADENA, CA 91125

EUGENE HERRIN
SOUTHERN METHODIST UNIVERSITY
DEPT. OF GEOLOGICAL SCIENCES
DALLAS, TX 75275-0395

ROBERT HERRMANN
ST. LOUIS UNIVERSITY
DEPT. OF EARTH & ATMOS. SCIENCES
3507 LACLEDE AVENUE
ST. LOUIS, MO 63103

VINDELL HSU
HQ/AFTAC/TTR
1030 S. HIGHWAY A1A
PATRICK AFB, FL 32925-3002

RONG-SONG JIH
DTRA/PMA
45045 AVIATION DRIVE
DULLES, VA 20166-7517

THOMAS JORDAN
MASS. INST. OF TECHNOLOGY
BLDG 54-918
CAMBRIDGE, MA 02139

LAWRENCE LIVERMORE NAT'L LAB
ATTN: TECHNICAL STAFF (PLS ROUTE)
PO BOX 808, MS L-208
LIVERMORE, CA 94551

LAWRENCE LIVERMORE NAT'L LAB
ATTN: TECHNICAL STAFF (PLS ROUTE)
PO BOX 808, MS L-205
LIVERMORE, CA 94551

LAWRENCE LIVERMORE NAT'L LAB
ATTN: TECHNICAL STAFF (PLS ROUTE)
PO BOX 808, MS L-200
LIVERMORE, CA 94551

THORNE LAY
UNIV. OF CALIFORNIA, SANTA CRUZ
EARTH SCIENCES DEPARTMENT
EARTH & MARINE SCIENCE BUILDING
SANTA CRUZ, CA 95064

ANATOLI L. LEVSHIN
DEPARTMENT OF PHYSICS
UNIVERSITY OF COLORADO
CAMPUS BOX 390
BOULDER, CO 80309-0309

JAMES LEWKOWICZ
WESTON GEOPHYSICAL CORP.
325 WEST MAIN STREET
NORTHBORO, MA 01532

LOS ALAMOS NATIONAL LABORATORY
ATTN: TECHNICAL STAFF (PLS ROUTE)
PO BOX 1663, MS D460
LOS ALAMOS, NM 87545

LOS ALAMOS NATIONAL LABORATORY
ATTN: TECHNICAL STAFF (PLS ROUTE)
PO BOX 1663, MS F665
LOS ALAMOS, NM 87545

LOS ALAMOS NATIONAL LABORATORY
ATTN: TECHNICAL STAFF (PLS ROUTE)
PO BOX 1663, MS C335
LOS ALAMOS, NM 87545

GARY MCCARTOR
SOUTHERN METHODIST UNIVERSITY
DEPARTMENT OF PHYSICS
DALLAS, TX 75275-0395

KEITH MCLAUGHLIN
CENTER FOR MONITORING RESEARCH
SAIC
1300 N. 17TH STREET, SUITE 1450
ARLINGTON, VA 22209

BRIAN MITCHELL
DEPT OF EARTH & ATMOSPHERIC SCIENCES
ST. LOUIS UNIVERSITY
3507 LACLEDE AVENUE
ST. LOUIS, MO 63103

RICHARD MORROW
USACDA/IVI
320 21ST STREET, N.W.
WASHINGTON DC 20451

JOHN MURPHY
MAXWELL TECHNOLOGIES
11800 SUNRISE VALLEY DRIVE
SUITE 1212
RESTON, VA 22091

JAMES NI
NEW MEXICO STATE UNIVERSITY
DEPARTMENT OF PHYSICS
LAS CRUCES, NM 88003

ROBERT NORTH
CENTER FOR MONITORING RESEARCH
1300 N. 17th STREET, SUITE 1450
ARLINGTON, VA 22209

OFFICE OF THE SECRETARY OF DEFENSE
DDR&E
WASHINGTON DC 20330

JOHN ORCUTT
INST. OF GEOPH. & PLANETARY PHYSICS
UNIV. OF CALIFORNIA, SAN DIEGO
LA JOLLA, CA 92093

PACIFIC NORTHWEST NAT'L LAB
ATTN: TECHNICAL STAFF (PLS ROUTE)
PO BOX 999, MS K5-12
RICHLAND, WA 99352

FRANK PILOTTE
HQ AFTAC/TT
1030 S. HIGHWAY A1A
PATRICK AFB, FL 32925-3002

KEITH PRIESTLEY
DEPARTMENT OF EARTH SCIENCES
UNIVERSITY OF CAMBRIDGE
MADINGLEY RISE, MADINGLEY ROAD
CAMBRIDGE, CB3 OEZ UK

JAY PULLI
BBN SYSTEMS AND TECHNOLOGIES, INC.
1300 NORTH 17TH STREET
ROSSLYN, VA 22209

DELAINE REITER
WESTON GEOPHYSICAL CORP.
73 STANDISH ROAD
WATERTOWN, MA 0472

PAUL RICHARDS
COLUMBIA UNIVERSITY
LAMONT-DOHERTY EARTH OBSERV.
PALISADES, NY 10964

MICHAEL RITZWOLLER
DEPARTMENT OF PHYSICS
UNIVERSITY OF COLORADO
CAMPUS BOX 390
BOULDER, CO 80309-0309

DAVID RUSSELL
HQ AFTAC/TTR
1030 SOUTH HIGHWAY A1A
PATRICK AFB, FL 32925-3002

CHANDAN SAIKIA
WOOODWARD-CLYDE FED. SERVICES
566 EL DORADO ST., SUITE 100
PASADENA, CA 91101-2560

SANDIA NATIONAL LABORATORY
ATTN: TECHNICAL STAFF (PLS ROUTE)
DEPT. 5704
MS 0979, PO BOX 5800
ALBUQUERQUE, NM 87185-0979

SANDIA NATIONAL LABORATORY
ATTN: TECHNICAL STAFF (PLS ROUTE)
DEPT. 9311
MS 1159, PO BOX 5800
ALBUQUERQUE, NM 87185-1159

SANDIA NATIONAL LABORATORY
ATTN: TECHNICAL STAFF (PLS ROUTE)
DEPT. 5736
MS 0655, PO BOX 5800
ALBUQUERQUE, NM 87185-0655

AVI SHAPIRA
SEISMOLOGY DIVISION
IPRG
P.O.B. 2286 NOLON 58122 ISRAEL

MATTHEW SIBOL
ENSCO, INC.
445 PINEDA CT.
MELBOURNE, FL 32940

JEFFRY STEVENS
MAXWELL TECHNOLOGIES
8888 BALBOA AVE.
SAN DIEGO, CA 92123-1506

TACTEC
BATTELLE MEMORIAL INSTITUTE
505 KING AVENUE
COLUMBUS, OH 43201 (FINAL REPORT)

LAWRENCE TURNBULL
ACIS
DCI/ACIS
WASHINGTON DC 20505

FRANK VERNON
UNIV. OF CALIFORNIA, SAN DIEGO
SCRIPPS INST. OF OCEANOGRAPHY
9500 GILMAN DRIVE
LA JOLLA, CA 92093-0225

RU SHAN WU
UNIV. OF CALIFORNIA, SANTA CRUZ
EARTH SCIENCES DEPT.
1156 HIGH STREET
SANTA CRUZ, CA 95064

JAMES E. ZOLLWEG
BOISE STATE UNIVERSITY
GEOSCIENCES DEPT.
1910 UNIVERSITY DRIVE
BOISE, ID 83725

SANDIA NATIONAL LABORATORY
ATTN: TECHNICAL STAFF (PLS ROUTE)
DEPT. 5704
MS 0655, PO BOX 5800
ALBUQUERQUE, NM 87185-0655

THOMAS SERENO JR.
SAIC
10260 CAMPUS POINT DRIVE
SAN DIEGO, CA 92121

ROBERT SHUMWAY
410 MRAK HALL
DIVISION OF STATISTICS
UNIVERSITY OF CALIFORNIA
DAVIS, CA 95616-8671

DAVID SIMPSON
IRIS
1200 NEW YORK AVE., NW
SUITE 800
WASHINGTON DC 20005

BRIAN SULLIVAN
BOSTON COLLEGE
INSITUTE FOR SPACE RESEARCH
140 COMMONWEALTH AVENUE
CHESTNUT HILL, MA 02167

NAFI TOKSOZ
EARTH RESOURCES LABORATORY
M.I.T.
42 CARLTON STREET, E34-440
CAMBRIDGE, MA 02142

GREG VAN DER VINK
IRIS
1200 NEW YORK AVE., NW
SUITE 800
WASHINGTON DC 20005

TERRY WALLACE
UNIVERSITY OF ARIZONA
DEPARTMENT OF GEOSCIENCES
BUILDING #77
TUCSON, AZ 85721

JIAKANG XIE
COLUMBIA UNIVERSITY
LAMONT DOHERTY EARTH OBSERV.
ROUTE 9W
PALISADES, NY 10964